LAWRENCE
LIVERMORE
NATIONAL
LABORATORY

LLNL-JRNL-853504

Tarda and Tagish Lake: Samples from the same outer Solar System asteroid and implications for D- and P-type asteroids

D. L. Schrader, E. A. Cloutis, D. M. Applin, J. Davidson, Z. A. Torrano, D. Foustoukos, C. M. O'D. Alexander, K. J. Domanik, T. Nakamura, M. Matsuoka, T. J. Zega, G. A. Brennecka, J. Render

August 22, 2023

Geochimica et Cosmochimica Acta

Disclaimer

Tarda and Tagish Lake: Samples from the same outer Solar System asteroid and implications for D- and P-type asteroids

Devin L. Schrader[1], Edward A. Cloutis[2], Daniel M. Applin[2], Jemma Davidson[3], Zachary A. Torrano[4], Dionysis Foustoukos[4], Conel M. O'D. Alexander[4], Kenneth J. Domanik[5], Moe Matsuoka[6], Tomoki Nakamura[7], Thomas J. Zega[5], Gregory A. Brennecka[8], and Jan Render[8]

[1]Buseck Center for Meteorite Studies, School of Earth and Space Exploration, Arizona State University, Tempe, AZ 85287, USA.
[2]Department of Geography, University of Winnipeg, Winnipeg, Manitoba R3B 2E9, Canada.
[3]Astromaterials Research and Exploration Science (ARES) Division, XI2, NASA Johnson Space Center, Houston, TX, USA.
[4]Earth and Planets Laboratory, Carnegie Institution for Science, Washington, DC 20015, USA.
[5]Lunar and Planetary Laboratory, University of Arizona, Tucson, Arizona 85721, USA.
[6]Geological Survey of Japan, National Institute of Advanced Industrial Science and Technology (AIST), Tsukuba, Ibaraki 980-8578, Japan.
[7]Department of Earth Science, Faculty of Science, Tohoku University, Aoba, Sendai, Miyagi 980-8578, Japan.
[8]Nuclear and Chemical Sciences Division, Lawrence Livermore National Laboratory, Livermore CA 94550, USA.

submitted to *Geochimica et Cosmochimica Acta*
September 29th, 2023
GCA-D-23-00860 Revision 1 submitted April 5th, 2024, Revision 2 submitted July 9th, 2024

ORCID iD:
Devin L. Schrader: 0000-0001-5282-232X
Edward A. Cloutis: 0000-0001-7301-0929
Daniel M. Applin: 0000-0002-5170-2382
Jemma Davidson: 0000-0002-3725-2960
Zachary A. Torrano: 0000-0002-5246-4400
Dionysis Foustoukos: 0000-0001-8402-3717
Conel M. O'D. Alexander: 0000-0002-8558-1427
Kenneth J. Domanik: 0009-0002-0184-1816
Moe Matsuoka: 0000-0003-1091-3041
Tomoki Nakamura: 0000-0001-9525-4086
Thomas J. Zega: 0000-0002-9549-022X
Gregory A. Brennecka: 0000-0002-0852-5595
Jan Render: 0000-0002-6534-9129

*Corresponding author: Devin L. Schrader
Phone: 480-965-0720
Email: devin.schrader@asu.edu
Buseck Center for Meteorite Studies
School of Earth and Space Exploration
Arizona State University
PO Box 871404
Tempe AZ 85287, USA

Words: 10168 in main text
Figures: 17
Tables: 9 (with 4 Supplementary Material files)
Key Words: chondrite, Tarda, Tagish Lake, D-type, P-type, asteroids

Abstract

We report a comprehensive study of the ungrouped type 2 carbonaceous chondrite, Tarda, which fell in Morocco in 2020. This meteorite exhibits substantial similarities to Tagish Lake, Wisconsin Range 91600, and Meteorite Hills 00432, which are generally considered to have originated from a D-type asteroid(s). We constrain the compositions and petrologies of the materials present in a potential sample of a D-type asteroid by reporting the petrography, bulk chemical compositions, bulk H, C, N, Cr, and Ti isotopic compositions, reflectance spectra, and *in situ* chemical compositions of metals, sulfides, carbonates, and FeO-poor and FeO-rich chondrule silicates of Tarda. We also present new data for Tagish Lake. We then compare Tarda with the other Tagish Lake-like meteorites.

Tarda and Tagish Lake appear to be from the same parent body, as demonstrated by their similar petrologies (modal abundances, chondrule sizes), mineral compositions, bulk chemical and isotopic compositions, and reflectance spectra. While the two other Tagish Lake-like meteorites, Wisconsin Range 91600 and Meteorite Hills 00432, show some affinities to Tagish Lake and Tarda, they also share similar characteristics to the Mighei-like carbonaceous (CM) chondrites, warranting further study. Similarities in reflectance spectra suggest that P-type asteroids 65 Cybele and 76 Freia are potential parent bodies of Tarda and the Tagish Lake-like meteorites, or at least have similar surface materials. Since upcoming spacecraft missions will spectrally survey D-type, P-type, and C-type Trojan asteroids (NASA's Lucy) and spectrally study and return samples from Mars' moon Phobos (JAXA's Martian Moons eXploration mission), which is spectrally similar to D-type asteroids, these meteorites are of substantial scientific interest. Furthermore, since Tarda closely spectrally matches P-type asteroids (but compositionally matches the D-type asteroid like Tagish Lake meteorite), P-type and D-type asteroids may represent fragments of the same or similar parent bodies.

1. Introduction

Tarda is an ungrouped type 2 carbonaceous (C2-ung) chondrite that fell in Morocco on August 25th, 2020, near the village of Tarda (Gattacceca et al., 2021). Ungrouped chondrites are those that are not unequivocal matches to established meteorite groups, and may represent unique fragments of distinct parent asteroids. Sometimes, ungrouped chondrites exhibit affinities to other ungrouped chondrites, and a new meteorite grouplet (3 or 4 members) or group (5+ members) is formed (e.g., Weisberg et al., 2006; Metzler et al., 2021). The study of multiple members from the same meteorite group, potentially from a common parent asteroid, enables understanding of the differences between members of the group (e.g., distinct degrees of thermal, aqueous, and/or shock alteration) and the diversity of processes active in their parent body (e.g., Alexander et al., 2007, 2013; Cloutis et al., 2011a,b; Schrader et al., 2011, 2015; Davidson et al., 2019a,b).

Based on bulk isotopic compositional similarities and noble gas compositions, Tarda was shown to be similar to the C2-ung Tagish Lake and the Tagish Lake-like meteorites Wisconsin Range (WIS) 91600 and Meteorite Hills (MET) 00432 (e.g., Hiroi et al., 2005; Moriarty et al., 2009; Nakamura et al., 2013; Yamanobe et al., 2018; Ushikubo and Kimura, 2021; Marrocchi et al., 2021; Avice et al., 2022; Hopp et al., 2022; Yesiltas et al., 2022; Yokoyama et al., 2023). Due to their 350–2500 nm spectral reflectance properties, such as albedo, spectral slope, and visible region spectral shape, these Tagish Lake-like meteorites have been proposed to be samples from a D-type asteroid(s), which potentially formed in the outer Solar System between 8 and 13 AU (Hiroi et al., 2005; Marrocchi et al., 2021; Yamanobe et al., 2018; Bryson et al., 2020). As these are the only meteorites thought to originate from D-type asteroids, they are of great scientific interest and highly relevant to upcoming spacecraft missions.

NASA's Lucy spacecraft is due to spectrally survey D-type Trojan asteroids (e.g., Levison et al., 2021), and JAXA's Martian Moons eXploration (MMX) mission is scheduled to collect both spectra and samples from Mars' moon Phobos, which is spectrally similar to D-type asteroids (Nakamura et al., 2021; Kuramoto et al., 2022). Having potential D-type asteroid or related material for study in the laboratory will be invaluable for interpretation of data from these spacecraft missions.

Recent studies have shown Tarda to be a chemically and petrographically unequilibrated, rare and scientifically interesting meteorite, warranting further detailed study. The chemical and *in situ*

O-isotope compositions of three FeO-poor chondrules and three isolated olivine grains in the matrix, identification of the dominant minerals via X-ray diffraction, as well as the bulk chemical, H, C, and N isotopic compositions of Tarda were reported by Marrocchi et al. (2021). Chromium and Ti isotope analyses of Tarda concluded it is consistent with a carbonaceous chondrite (Hellmann et al., 2023; Yokoyama et al., 2023). Despite these initial studies, many fundamental parameters about Tarda (e.g., reflectance spectra, average chondrule size and petrographic types, modal mineralogy, chemical compositions of FeO-rich silicates, sulfides, metal, and carbonates) are not known in the literature. Therefore, Tarda and other meteorites considered similar to Tagish Lake cannot be fully compared to one another with the available literature data.

To constrain the composition and petrology of this rare material and its components, and to provide insights into the material present on D-type asteroids, we discuss the petrography, bulk H, C, N, Cr, and Ti isotopic compositions, bulk chemical compositions, reflectance spectra, and *in situ* chemical compositions of metals, sulfides, carbonates, and FeO-poor and FeO-rich chondrule silicates of Tarda and compare them to the other Tagish Lake-like meteorites, primarily Tagish Lake.

2. Samples and Analytical Procedures

2.1. Mineralogy and petrology

The stones belonging to the Tarda meteorite shower are often sub-cm in size, fully to partially fusion crusted, with charcoal black interiors containing small (<0.5 mm) off-white rounded to irregular shaped objects (Fig. 1). All samples of Tarda studied here were kept in dry N_2 purged desiccator cabinets in the Buseck Center for Meteorite Studies at Arizona State University (ASU) after arriving on September 8th, 2020. The samples were, therefore, isolated from the terrestrial atmosphere from that point on until preparation of the various samples for analysis.

We analyzed two polished mounts of Tarda prepared from two separate stones (ASU2149_C1 and ASU2149_C2) that were collected within days of the fall. We also analyzed a polished mount of Tagish Lake (ASU1684_C1) for comparison (Fig. 2; see Table 1 for sample sizes). High-resolution backscattered electron (BSE) imaging (e.g., Figs. 2–4), X-ray element mapping, and initial mineral identification via energy dispersive X-ray spectroscopy (EDS) were conducted on C-coated polished mounts using the JEOL-8530F Hyperprobe electron probe microanalyzer

(EPMA) at ASU and the Cameca SX-100 EPMA at the University of Arizona (UA) (Supplementary Material [SM] 1). Apparent (2D) chondrule sizes were measured from BSE images and X-ray maps using Adobe Photoshop® (Table 1 and SM 2). The chondrule sizes reported here are the apparent (2D) mean diameters, which have been found to be the same as 3D sizes within uncertainty (e.g., Metzler, 2018; Metzler et al., 2019), and are directly comparable to other studies that also report apparent (2D) chondrule sizes (e.g., Zolensky et al., 2002; Blinova et al., 2014).

The modal mineralogies of Tarda (ASU2149_C1 and ASU2149_C2) and Tagish Lake (ASU1684_C1) were determined using digital point counting (e.g., Schrader et al., 2014; Donaldson Hanna et al., 2019). Backscattered electron images and X-ray element maps (Ca, Fe, Mg, Na, S, Al, K, Ni, Si, Ti, Co, Cr, Mn, and P) were obtained with the EPMA instruments at ASU and UA (operating conditions: 15.0 keV and 40.0 nA). We measured the modal abundances of chondrules and fine-grained matrix (Table 2), as well as those of individual mineral phases by pixel counting (i.e., digital point counting) with Adobe Photoshop® (n.b., area % determined by point counting can be assumed to be equivalent to vol.%; e.g., Eisenhour, 1996). In doing so, we obtained modal abundances of olivine, pyroxene, plagioclase, Al-spinel, Ca-carbonate, phosphate, chromite, Fe,Ni metal, magnetite, and sulfide (Table 2). We measured the pixels corresponding to each mineral ten times, with the uncertainty in the mean value being the standard deviation of the mean. We propagated uncertainties when the total abundances of measured minerals were determined (Table 2). The cumulative totals of identified minerals measured in Tarda and Tagish Lake do not sum to 100 vol.% (Table 2) for two reasons. One, all modal abundance estimates of minerals are lower limits since they do not include fine-grained material below the resolution of the X-ray element maps (especially in the fine-grained interchondrule matrix). Secondly, identifying minerals via image analysis is unable to locate phyllosilicates and amorphous silicates confidently (e.g., Donaldson Hanna et al., 2019). Since the difference from 100 vol.% is nearly equivalent to the matrix abundances in each meteorite (Table 2), this confirms the unidentified vol.% is due to fine-grained phyllosilicate-rich matrix in Tarda and Tagish Lake.

The quantitative chemical compositions of chondrule olivine, metals, sulfides, and carbonates were obtained via wavelength-dispersive X-ray spectroscopy (WDS) with the Cameca SX-100 EPMA at UA (Tables 3–5 and SM 3), using a focused beam for individual points and line scans, with operating conditions of 15 keV and 20 nA for olivine, metals, and sulfides, and 15 keV and

8 nA for carbonates, and a PAP correction method (a Phi-Rho-Z correction technique). Peak and background counting times varied per element to optimize detection limits; standards and detection limits are listed in Tables 3–5 and SM 3. In addition to Tarda and Tagish Lake, to help determine if compositional comparison can be used to distinguish between meteorite types, we also analyzed carbonates via WDS in a thin section of the Ivuna-like carbonaceous (CI) chondrite Orgueil USNM6765-2 and two polished mounts of the Mighei-like carbonaceous (CM) chondrite Kolang (ASU2147_C1 [the CM1/2 host] and ASU2147_C3c [a clast of CM1 material]).

2.2. Bulk sample analyses: Compositions, isotopes, and reflectance spectra

Interior chips of Tarda (total of 1.03 g), that contained no fusion crust, were powdered at ASU to create a uniform sample and used to obtain: (1) bulk H, C, and N abundances and isotopic compositions, (2) bulk Cr and Ti isotopic compositions (mass-independent variations of nucleosynthetic origin), (3) bulk elemental compositions, and (4) reflectance spectra. For comparison to the powder of Tarda, the reflectance spectra of a 0.2384 g fusion crust-free chip of Tarda (ASU2149) (~0.5 × 1 cm) was also analyzed.

2.2.1. Bulk H, C, and N abundances and isotopic compositions

Because the H, C, and N elemental abundances and isotopic compositions are known to vary between meteorite groups (e.g., Alexander et al., 2012, 2013; Vacher et al., 2020; Marrocchi et al., 2021, 2023), an aliquot of the Tarda homogenized powder was analyzed for these elements at the Earth and Planets Laboratory (EPL) of the Carnegie Institution for Science.

The C and N elemental abundances and isotopic compositions of the homogenized powders were measured with a Thermo Scientific Delta V^{Plus} mass spectrometer interfaced with a Carlo Erba (NA 2500) elemental analyzer via a Conflo III interface. For H analyses, we used a Thermo Finnigan $Delta^{Plus}$ XL mass spectrometer connected to a Thermo Finnigan Thermal Conversion elemental analyzer (TC/EA) operating at 1400°C. N_2 and CO_2 references gases were introduced via the Conflo III, while a dual inlet system facilitated the use of a H_2 reference gas of known δD value (–123.39 ‰ SMOW) (Alexander et al., 2007; Foustoukos et al., 2021). Internal working gas standards were analyzed at regular intervals during a run to monitor the internal precision of the measured isotopic ratios and elemental abundances. In-house standards, which included both liquid and solid materials, were also analyzed at regular intervals between samples to calibrate and

correct the data. The in-house standards are calibrated against international (Standard Mean Ocean Water, SMOW, National Bureau of Standards-22, Pee Dee Belemnite, and air) and other certified standards from the Isoanalytical Laboratory, the US Geological Survey, the National Bureau of Standards, and the Oztech Trading Company. A H_3^+ correction was determined and applied to the H measurements (Sessions et al., 2001). The reported uncertainties for the elemental and isotopic analyses correspond to 1σ deviations based either on replicate analyses of standards or analyses of at least two aliquots of individual samples, whichever is the larger. A total of one and two aliquots were analyzed for C-N and H, respectively.

The samples Tarda were kept in dry N_2 purged desiccator cabinets from September 8th, 2020, at ASU, prior powdering and shipping to EPL for analysis in April 2021. After weighing ~2 mg aliquots into Ag boats for H analysis and a ~8 mg sample into a Sn boat for C and N analysis, the samples were stored in a desiccator until their analyses. They were also reweighed after several days in the desiccator. Before H analysis, the samples were transferred to a zero-blank autosampler and flushed with dry He for at least one hour to minimize the amount of water absorbed from the atmosphere (Alexander et al., 2010). The two replicates of each sample were analyzed sequentially to check for sample heterogeneity and small memory effects on the δD measurements known to occur with D-enriched samples (e.g., Alexander et al., 2007, 2012). The H abundances of the duplicate samples generally differed by ≤ 1 % of their absolute values, and the δD values differed by a median of 18 ‰ (the δ notation stands for the deviation of a sample ratio from a standard ratio in parts per thousand, $\delta=(R_{smp}/R_{std}-1) \times 1000$ and in this case R=D/H). Blanks were run between different samples to reduce the memory effects. Memory effects were also monitored by analyzing in-house standards of H-bearing solids during the course of an analytical run. There is no memory effect for the C and N analyses (Alexander et al., 2012).

2.2.2. Sample processing for bulk elemental and Cr and Ti isotopic analysis

The homogenized Tarda sample powder, and the Allende, BCR-2 and DTS-1 reference powders were dissolved in 4 mL of a 1:1 mixture of concentrated HNO_3 and HF in a 15 mL Savillex Teflon beaker and heated on a hot plate at approximately 120ºC for 48 hours at EPL. The solutions were then dried and redissolved in 2 mL of a 2:1 mixture of concentrated HF and HNO_3 and transferred to 3mL Savillex Teflon beakers that were then each placed in a Teflon jacket within a metal Parr® digestion bomb and heated in an oven at 190 ºC for 96 hours. Next, each sample

was transferred back into 15 mL Savillex Teflon beakers and dried before being treated with 250 µL of concentrated HNO_3, dried, and treated with 250 µL of concentrated HCl. The samples were then dried and treated with 2 mL of 6 M HCl and placed capped on a hot plate for 96 hours to eliminate fluorides. The Parr® bomb digestion and sample treatment procedures were repeated three times with complete evaporation of the acid mixture between each step to ensure complete dissolution of the sample.

2.2.3. Bulk elemental analysis

The bulk major and trace element concentrations of Tarda were measured using the Thermo Scientific iCAP-Q quadrupole inductively coupled plasma mass spectrometer (Q-ICPMS) at EPL. A synthetic solution with similar concentration to the samples, an Allende (CV3) Smithsonian Reference Material solution, and a BCR-2 geological reference material solution were measured regularly alongside samples to assess measurement accuracy and precision, and based on these measurements we estimate an analytical uncertainty of ±10% for all elements.

2.2.4. Bulk Cr and Ti isotopic analysis

Mass-independent Cr and Ti isotopic compositions were analyzed for the bulk sample of Tarda (from the 1.03 g homogenized powder sample) to determine the nucleosynthetic character of the material.

2.2.4.1. Cr and Ti elemental separation chemistry

Chromium was separated from the sample matrix using a three-column separation procedure (Torrano et al., 2021). The column chemistry methods described by Torrano et al. (2021) were optimized for multi-collector inductively coupled plasma mass spectrometry (MC-ICPMS) measurements, so some modifications were made in preparation for the thermal ionization mass spectrometry (TIMS) methods used in this study. Specifically, our testing found that TIMS methods are especially sensitive to the presence of even very minor amounts of Mg and Ca in the purified Cr solution leading to the potential for impaired ionization. To remedy this, the second column in the Torrano et al. (2021) procedure was repeated 2–4 times until the Cr elution solution dried to a small, green dot rather than a white or pink dot, indicating complete removal of matrix elements. The Cr yields of all samples exceeded 90% and the average total procedural blank was

less than 2 ng of Cr, which is insignificant compared to the approximately 20 µg of Cr purified from each sample. Titanium was separated from the sample matrix using a two-column separation procedure (Torrano et al., 2019). The Ti yields of all samples exceeded 98% and the total procedural blank was less than 1 ng of Ti, which is insignificant compared to the approximately 10 µg of Ti purified from each sample. Cr and Ti isotope analyses were obtained from the same dissolved sample aliquot.

2.2.4.2. Cr isotope analyses

The Cr isotopic composition of Tarda, as well as the standards DTS-1 and Allende, were measured using the Thermo Triton XT TIMS at EPL. Purified Cr sample solution was loaded onto the middle third of pre-degassed zone-refined Re filaments in a few microliters of 3M HCl between melted Parafilm dams in a single filament assembly. Equal volumes of Al_2O_3-doped silica gel and saturated boric acid were added to the filament following the Cr sample drops and the mixtures were dried on the filament at a current of 0.6 A. Once dry, the current was increased slowly to ~2 A until the filaments glowed red for a second before being turned down. Approximately 3 µg of Cr was loaded onto each filament, and 4 filaments were loaded per sample for a total of 12 µg of Cr measured for per sample. A filament loaded with 3 µg of the NIST SRM 979 Cr isotopic standard loaded in the same manner as the sample filaments was run before and after each sample filament. Each filament analysis consisted of 40 blocks of 30 ratios for a total of 1200 ratios per analysis, with an 8 s integration time for each ratio. The intensities of ^{50}Cr, ^{52}Cr, ^{53}Cr and ^{54}Cr were measured along with ^{48}Ti, ^{51}V, and ^{56}Fe to correct for isobaric interferences. The beam intensity was typically 10 V for ^{52}Cr. Data were corrected for instrumental mass fractionation using an exponential mass fractionation law and a $^{50}Cr/^{52}Cr$ ratio of 0.051859 (Shields et al., 1966). The $^{53}Cr/^{52}Cr$ and $^{54}Cr/^{52}Cr$ ratios are expressed in ε-notation, which is a parts per 10,000 deviation from the NIST SRM 979 Cr isotopic standard. Based on repeated measurements of standards run during these analyses, we estimate an external reproducibility (2SD) of ±0.12 for $\varepsilon^{53}Cr$ and ±0.18 for $\varepsilon^{54}Cr$.

2.2.4.3. Ti isotope analyses

The Ti isotopic compositions of samples were determined as outlined in Render et al. (2019) with minor adjustments. After chemical purification (§2.2.4.1), interfering elements were far

below the maximum thresholds determined by Zhang et al. (2011) [max V/Ti = 0.00018, Cr/Ti = 0.0012, and Ca/Ti = 0.006]. Titanium isotopic measurements were performed employing the Neptune *Plus* MC-ICPMS and a Cetac Aridus II® desolvating introduction system at the Lawrence Livermore National Laboratory. Using a Jet sampler and X skimmer cones, this setup resulted in intensities for ^{48}Ti between 35 and 40 V in medium resolution for 700 ppb Ti solutions (corresponding to a total ion beam intensity of 4.7 to 5.2×10^{-10} A). Due to the large relative axial spread of the atomic masses from ^{44}Ca to ^{53}Cr, it was necessary to determine the Ti isotope ratios in two lines, where the first line encompasses masses 44 to 50 and the second line measures atomic masses 49, 51, and 53 to correct for minor isobaric interferences from Cr and V. Each measurement consisted of a 30 s baseline as well as 30 cycles of 8.3 s and 2.1 s integration times for the first and second line, respectively, transitioned by 3 s idle time. All masses (44, 46, 47, 48, 49, 50, 51 and 53) were monitored using 10^{11} Ω amplifiers. Because Ti isotope measurements can suffer from a polyatomic interference on atomic mass 50 (presumably $^{36}Ar^{14}N^{+}$), the measurements were performed on the left shoulder of the peak plateau to avoid the polyatomic interference. Based on repeated measurements of standards run during these analyses, we estimate an external reproducibility (2SD) of ±0.27 for ε^{46}Ti, ±0.09 for ε^{48}Ti, and ±0.31 for ε^{50}Ti. Isotope data were corrected for mass-bias by internal normalization to ^{49}Ti/^{47}Ti = 0.749766 using the exponential law and are reported in ε-notation relative to the Origins Lab OL-Ti standard:

$$\varepsilon^{i}Ti = \left[\frac{\left(^{i}Ti/^{47}Ti\right)_{sample}}{\left(^{i}Ti/^{47}Ti\right)_{standard}} - 1\right] \times 10^{4}$$

2.2.5. Reflectance spectra

We analyzed an aliquot of fine-grained but unsorted Tarda powder (0.51 g) made from the 1.03 g of homogenized, fusion crust-free fragments that was used in this study for all other bulk compositions (H-C-N isotopes and abundances, Cr and Ti isotopes, and bulk elemental composition). We also spectrally characterized a 0.2384 g fusion crust-free chip of Tarda.

Reflectance spectra from 350 nm to 2500 nm were measured relative to a calibrated Fluorilon standard with an Analytical Spectral Devices LabSpec4 Hi-Res spectrometer at i=30°, e=0°, at ambient pressure and temperature (SM 4). Reflectance spectra from both the fine unsorted powder and small, flat chip of the stone were collected at the University of Winnipeg. The powder was packed into an Al sample cup by first gently pouring, then tapping the cup several times, and

finally scraping the excess off with a glass slide held away from the sample at 45°. The powder was repacked in its sample cup three times, and no significant variation in the reflectance spectra was observed. The field of view for all measurements was roughly 4 mm in diameter, and the light source used was an in-house 150 W quartz-tungsten halogen operated at 110 W and collimated to a divergence of <1.5°. The spectra have between 2 and 7 nm resolution with 1.4 nm spectral steps and the data is internally resampled by the instrument to output data at 1 nm intervals. A total of 1000 spectra of the white standard, dark current, and sample were collected to improve the signal to noise ratio of the data.

Continuum removal from the Tarda spectra, discussed in §4.1.6, was performed by constructing a straight line continuum tangent to the reflectance spectra in the 500 nm and 1800 nm regions and dividing the spectrum by this continuum, similar to how this procedure has been applied to other carbonaceous chondrite spectra (e.g., Cloutis et al., 2011a,b). While the choice of a continuum's tangent points can affect the depths and, to a lesser extent, positions of any absorption features, it has proven effective in previous analyses for enhancing the visibility of absorption features that have mineralogical significance (Cloutis et al., 2011a,b). This technique allows otherwise hard-to-see absorption bands to be accentuated and band centers to be determined, which can then be linked to specific phases (e.g., magnetite, phyllosilicates, and mafic silicates) that contribute to absorption in specific wavelength regions (Cloutis et al., 2011a,b). This technique has been successfully applied to determining what phases contribute to the reflectance spectra of other dark carbonaceous chondrites (Cloutis et al., 2011a,b).

Mid infrared spectra of the powder and the fusion crust-free chip were also measured, with a Bruker Vertex 70, using a SpecAc bidirectional accessory. These measurements were collected relative to Labsphere InfraGold in a purged dry-N_2 atmosphere, using a MCT detector and Globar light source. The sample preparation for these measurements was the same as those for the visible and near-infrared (VNIR) analyses, as was the viewing geometry of i=30° and e=0°.

Spectra collected on aliquots of Tagish Lake are included here, and the reader is referred elsewhere for experimental procedures (Hiroi et al., 2001; Izawa et al., 2015; Gilmour et al., 2019).

A reflectance spectrum ranging from 250 nm to 2500 nm of a rough surface of a MET 00432 chip sample was measured every 5 nm at Mizusawa Very Long Baseline Interferometer (VLBI) Observatory using the same instrument conditions as described in Yamada et al. (1999). The footprint size was ~2 mm × 3 mm. The spectrum was collected with a viewing geometry of i=30°

and e=0° relative to Labsphere Spectralon at ambient pressure and temperature, using a deuterium lamp (250 to 390 nm) and a halogen lamp (390 to 2500 nm) as light sources.

The reflectance spectra of WIS 91600 (<125 μm and <75 μm powders) were acquired from the RELAB public database (https://pds-geosciences.wustl.edu/spectrallibrary/default.htm) that were analyzed in Cloutis et al. (2012a). The WIS 91600 spectra were measured relative to a pressed halon powder white standard with a viewing geometry of i=30° and e=0° and 5 nm spectral resolution.

3. Results

3.1. Mineralogy and petrology

3.1.1. Tarda

The petrographies, modal abundances, and modal mineralogies of the two polished Tarda mounts (Figs. 2a,b) are very similar to one another (Tables 1 and 2), and their *in situ* mineral compositions are indistinguishable (Tables 3–5 and SM 3). Therefore, mineral compositions and petrographic observations are presented together. Tarda contains ~0.2 vol.% calcium-aluminum-rich inclusions (CAIs), ~6.5 vol.% chondrules and 93.3 vol.% matrix (total sample area 51.3 mm^2). The minerals identified in Tarda from X-ray element map analysis (confirmed with EDS) include olivine (~3.3 vol.%), dolomite (~3.2 vol.%), magnetite (~4.1 vol.%), Fe-sulfide (~2.4 vol.%; pyrrhotite and pentlandite), phosphate (~0.15 vol.%), and trace amounts (<0.01 vol.%) of chromite, Fe,Ni metal, and Al-spinel, with the remaining material being phyllosilicates (~86.9 vol.%) (Table 2). We identified 21 whole chondrules, 18 FeO-poor (one dusty olivine and 17 type I; mean Fe/[Fe+Mg] atomic ratio <10%) and three FeO-rich (type II; mean Fe/[Fe+Mg] atomic ratio >10%) chondrules, all of which are porphyritic (Table 1) and highly aqueously altered (olivine phenocrysts partially replaced by phyllosilicates and no remaining unaltered glass). For example, one FeO-rich chondrule is partially replaced by phyllosilicates (Fig. 3e,f), while another is almost completely replaced by phyllosilicates (Fig. 3h). FeO-rich chondrules are significantly less abundant than FeO-poor chondrules (e.g., Figs. 2a,b). The range of apparent (2D) diameters of the 21 chondrules is 0.07–1.30 mm (mean 0.26±0.12 mm; ±2SE). Numerous FeO-poor olivine fragments were observed in the matrix; while they are most likely chondrule fragments, their sizes are not included in the chondrule size determination as they are not whole chondrules. The range

of chondrule olivine compositions is $Fa_{0.5–55.6}$ with at.% Fe/Mn ratios of 4 to 134 (# analyses = n = 87; 10 chondrules [7 FeO-poor, including 1 dusty olivine chondrule, and 3 FeO-rich chondrules; SM 3]). The Fe-sulfides observed include both Ni-poor (<1 wt.% Ni) Fe-depleted pyrrhotite (mean Fe/S at.% ratio = 0.87, n= 14) and pentlandite (n = 22) (Fig. 3g). Nickel-rich pyrrhotite was also observed (n = 15) but may result from EPMA beam overlap with pentlandite. Rare Fe,Ni metal in an FeO-poor chondrule has Ni = 5.6–6.2 wt.% and Co = 0.20–0.24 wt.% (n = 2; Table 4).

3.1.2. Tagish Lake

The Tagish Lake sample studied here (Fig. 2c) most closely resembles the carbonate-rich lithology described by Zolensky et al. (2002) and Nakamura et al. (2003). Tagish Lake contains ~0.3 vol.% CAIs, ~5.9 vol.% chondrules and 93.8 vol.% matrix (total sample area 125.4 mm^2). This chondrule abundance is lower than some samples studied by Blinova et al. (2014), but is similar to the ~5 vol.% chondrules observed in the 'Tagish Lake 11i' sample. The minerals identified in Tagish Lake from X-ray element map analysis (confirmed with EDS) include olivine (~4.1 vol.%), Ca-carbonate (~3.2 vol.%; dolomite and calcite), magnetite (~4.6 vol.%), Fe-sulfide (~1.9 vol.%; pyrrhotite and pentlandite), Al-spinel (~0.02 vol.%) and trace amounts (<0.01 vol.%) of phosphate, chromite, and Fe,Ni metal, with the remaining material being phyllosilicates (~86.2 vol.%) (Table 2). We identified 57 whole chondrules, 52 FeO-poor chondrules and five FeO-rich chondrules (e.g., Figs. 2c and 4). The apparent (2D) diameters of these 57 chondrules range from 0.05 to 1.37 mm (mean 0.29±0.05 mm; ±2SE). The chondrules are heavily aqueously altered and the majority are porphyritic; only two barred olivine chondrules and one cryptocrystalline chondrule were observed (Table 1 and Fig. 4a). Some chondrules have fine-grained rims, and cracks normal to the chondrule surfaces are sometimes present in the fine-grained rim (e.g., Fig. 4e), like that observed by Mouti Al-Hashimi et al. (2023) in CM chondrites. The range of chondrule olivine compositions is $Fa_{0.6–54.3}$ with at.% Fe/Mn ratios of 5 to 142 (n = 97). The Fe-sulfides observed include Ni-rich (1<Ni<16 wt.%) Fe-depleted pyrrhotite (Ni is potentially from beam overlaps with pentlandite, n = 28) and pentlandite (n = 14). Since all pyrrhotite analyzed had greater than 1 wt.% Ni, no Ni-poor (<1 wt.% Ni) pyrrhotite was observed that could be used to determine the at.% Fe/S ratio using the technique of Schrader et al. (2021).

3.2. Bulk isotopic and elemental compositions

Tarda has a bulk isotopic and elemental composition of $\delta^{13}C$ = 8.0±0.4‰ (4.17±0.03 wt.% C), $\delta^{15}N$ = 62.0±0.2‰ (0.297±0.003 wt.% N), and δD = 608±18‰ (0.92±0.01 wt.% H) (all uncertainties are 1σ), yielding a bulk C/H (wt.%) ratio of 4.55 (Table 6). The Cr and Ti isotopic compositions are $\varepsilon^{53}Cr$ = 0.02±0.14, $\varepsilon^{54}Cr$ = 1.14±0.17, $\varepsilon^{46}Ti$ = 0.55±0.10, $\varepsilon^{48}Ti$ = –0.06±0.03, and $\varepsilon^{50}Ti$ = 2.94±0.13 (all uncertainties are 2SE; n = 5) (Tables 7 and 8). The USGS standard DTS-1 and our aliquot of Allende yielded $\varepsilon^{i}Cr$ values that are indistinguishable from those previously reported for these samples (e.g., Trinquier et al., 2007; Williams et al., 2020; Torrano et al., 2021; Zhu et al., 2021; Table 7). The USGS standard BCR-2 and our aliquot of Allende yield $\varepsilon^{i}Ti$ values that are also indistinguishable from those previously reported for these samples (e.g., Zhang et al., 2011; Gerber et al., 2017), demonstrating the accuracy of our method (Table 7). The bulk elemental abundances in Tarda are given in Table 9, and are discussed in §4.1.2.

3.3. Reflectance spectra

The 350–5000 nm reflectance spectra of the Tarda meteorite powder and chip show overall low reflectance (<0.03 in the visible region for the powder), a relatively strong spectral red slope, a concave-down shape below ~500 nm, and a flat to slightly-concave-up shape between ~500 nm and 2500 nm (Fig. 5). Both spectra exhibit a weak and narrow absorption feature near 430 nm, a strong absorption feature in the ~2.7–3.1 μm region, and weaker absorption features in the 3.4 μm and 4 μm regions.

The chip and powder spectra of Tarda are similar, differing mostly in terms of overall reflectance (Fig. 5). The scattering properties of chips and powders differ due to their solid versus porous nature, and differences in reflectance between chips and powders are normal (Cloutis et al., 2018). The narrow absorption band near 430 nm is associated with a spin-forbidden absorption due to ferric Fe, likely in a tetrahedrally-coordinated site in phyllosilicates (Greenberger et al., 2015). There are suggestions of an absorption feature near 2300 nm that could be attributed to various components of Tarda, such as carbonate (Gaffey, 1986), aliphatic organics (Cloutis et al., 1994), or Mg-OH in phyllosilicates (Clark et al., 1990).

The absorption feature near 2.71 μm is attributed to stretching vibrations in OH that is present in Tarda's phyllosilicates, while the longer-wavelength shoulder, centered near 3 μm, is attributable to stretching vibrations of H_2O and the first overtone of H_2O bending vibrations, likely due to H_2O present in saponitic phyllosilicates (Clark et al., 1990). The 3.3 μm region absorption

feature is likely due to carbonates and/or aliphatic-bearing organics (e.g., Bellamy et al., 1958; Adler and Kerr, 1963a,b). The 4 μm region band is due to carbonates, as aliphatic organics do not have an absorption feature in this region.

4. Discussion

4.1. Tarda and Tagish Lake: Meteorites from the same parent asteroid?

4.1.1. Modal mineralogies

The abundances of major minerals, chondrules, CAIs, matrix and phyllosilicates in Tarda are very similar to those of Tagish Lake (Table 2). The mineral abundances in both Tarda and Tagish Lake are unlike those observed by Donaldson Hanna et al. (2019) for CI, CM1/2, CM2, type 3 Vigarano-like carbonaceous (CV), and the type 2 Renazzo-like carbonaceous (CR) chondrites. We use the abundances in Donaldson Hanna et al. (2019) as they were determined by the same technique used here and are thus directly comparable. Tarda and Tagish Lake most closely resemble the CM1/2 and CI chondrites, although Tarda and Tagish Lake (~3.3 and ~4.1 vol.%, respectively) contain more olivine than the CI Orgueil (~0.03 vol.% olivine) and the CM1/2 ALH 83100 (~0.20 vol.% olivine), but less than the CM2 Murchison (11.3 vol.% olivine) (Table 2; Donaldson Hanna et al., 2019). Tarda and Tagish Lake also contain lower estimated phyllosilicate abundances (~86.9 and ~86.2 vol.%, respectively) than the CI Orgueil (~96.7 vol.%) and the CM1/2 ALH 83100 (95.7 vol.%), but more than the CM2 Murchison (~74.5 vol.% phyllosilicates; Donaldson Hanna et al., 2019). The abundances of chondrules and matrix in the Tarda and Tagish Lake samples studied here are also similar to one another, but unlike those of recognized chondrite groups (e.g., see meteorite group abundances in Table 2 of Weisberg et al., 2006). Tagish Lake is known to contain multiple lithologies, and these distinct lithologies are known to contain chondrule abundances between 5 vol.% and 40 vol.% (Blinova et al., 2014). Therefore, based on the modal abundances of components and minerals within Tarda and Tagish Lake studied here, we find they are similar to one another and unlike known meteorite groups.

4.1.2. Bulk isotopic and elemental compositions

Bulk isotopic and elemental compositions indicate that Tarda is very similar to Tagish Lake (Figs. 6–8; e.g., Brown et al., 2000; Trinquier et al., 2009; Petitat et al., 2011; Alexander et al., 2012; Marrocchi et al., 2021). The H, C, and N compositions of Tarda determined here are consistent with those reported by Marrocchi et al. (2021) (Table 6; Fig. 6), and of the bulk meteorite compositions analyzed using the same protocols are most similar to those of Tagish Lake (e.g., Alexander et al., 2012). It is important to note that our H, C, and N compositions for Tarda are similar to those of Marrocchi et al. (2021), despite using different samples of Tarda, analytical equipment, and methods. The method in Marrocchi et al. (2021) used a pre-degassing technique (48 hours at 120° C; developed by Vacher et al., 2020) ideally to remove terrestrially adsorbed water from the sample. Vacher et al. (2020) found that for CI chondrites analyzed with this pre-degassing technique, the abundance of H was up to a factor of two lower than values reported by Alexander et al. (2012), potentially supporting their argument for removal of terrestrial water. Using stepwise pyrolysis technique, Lee et al. (2023) found that terrestrially adsorbed water from the atmosphere contaminated CM chondrite falls. Since Tarda is an extensively aqueously altered carbonaceous chondrite meteorite fall, terrestrially adsorbed water may at first seem to be of concern for the Tarda sample analyzed here. However, Garvie et al. (2024) found that carbonaceous chondrite samples (including Tarda) stored in dry N_2 purged desiccator cabinets had significantly less adsorbed water than samples stored in atmosphere, and our sample of Tarda was stored in the same N_2 purged desiccator cabinets. In addition, despite using the method of Alexander (2012), our data for Tarda has a lower H abundance than Tarda samples analyzed by Marrocchi et al. (2021) (Table 6; Fig. 6). Therefore, our sample of Tarda is not noticeably contaminated by terrestrial water, which is supported by its similar H, C, and N abundances and isotopic compositions (Table 6; Fig. 6).

The bulk H concentration (wt.%) and δD value (‰) of Tarda are also near those of CR chondrites (Fig. 6a), but the higher C/H ratio (Fig. 6b) and lower $\delta^{15}N$ (‰) value compared to CR chondrites (Fig. 6c) indicates that Tarda and the CRs are not related. In addition, the *in situ* O-isotope compositions of FeO-poor chondrule olivines in Tarda are distinct from those of FeO-poor chondrule olivines in CR chondrite chondrules (Schrader et al., 2013, 2017, 2018a, 2020; Tenner et al., 2015, 2018; Marrocchi et al., 2021; Pinto et al., 2024). The bulk O isotope composition and mass-independent Cr and Ti isotopic compositions of Tarda are also most similar to Tagish Lake (Table 8 and Fig. 7). The Cr and Ti isotope variations amongst Solar System materials have been

proposed to result from the heterogeneous distribution of isotopically anomalous presolar dust in the protoplanetary disk, making them excellent tracers of genetic relationships among Solar System reservoirs or meteorite parent bodies (e.g., Trinquier et al., 2009; Warren, 2011; Torrano et al., 2021; Render et al., 2022; Zhu et al., 2023; Rüfenacht et al., 2023). While the ε^{54}Cr and ε^{50}Ti compositions of Tarda overlap with the field for CM chondrites (Fig. 7a), the Δ^{17}O (‰) vs. ε^{54}Cr and Δ^{17}O (‰) vs. ε^{50}Ti compositions (Figs. 7b,c; this study, Grossman, 2000; Trinquier et al., 2009; Petitat et al., 2011; Gattacceca et al., 2021) are unlike those of CM chondrites. These isotopic compositions are distinct from other meteorite groups and ungrouped carbonaceous chondrites, suggesting that Tarda and Tagish Lake are genetically related (e.g., Marrocchi et al., 2021), or at least formed from materials with similar compositions that potentially formed spatially and temporally close to one another in the protoplanetary disk. The Xe and Fe isotopic compositions of Tagish Lake and Tarda have also been shown to be very similar to one another, but distinct from that of CI chondrites and asteroid Ryugu, suggesting that Tarda and Tagish Lake are not related to CI chondrites (Avice et al., 2022; Hopp et al., 2022).

The bulk and trace element compositions of Tarda determined here (Table 9), are similar to the bulk compositions of two Tarda aliquots determined by Marrocchi et al. (2021). Tarda shows a similar bulk composition to that of Tagish Lake (Brown et al., 2000), comparable to the findings of Marrocchi et al. (2021). The lithophile element abundances of Tarda are very similar to those of CI chondrites, for Al, Sc, Ca, La, Sm, Eu, Yb, and V (Figs. 8a,b). However, there are depletions, relative to CI, for the moderately volatile lithophiles Cr, Mn, and K (Figs. 8c,d) and for siderophile and chalcophile elements. Tarda's lithophile, siderophile, and chalcophile elements (Fig. 8) are most like those of CM chondrites (Lodders et al., 2021), Tagish Lake (Brown et al., 2000), and WIS 91600 (Choe et al., 2010).

4.1.3. Sulfide and Fe,Ni metal chemical compositions

The chemical compositions of pyrrhotite and pentlandite in a meteorite can provide information about the formation conditions of the host rock, such as the equilibration temperature at which those compositions formed (e.g., Jamsja and Ruzicka, 2010; Berger et al., 2011; Schrader et al., 2015; 2016; 2018b; Davidson et al., 2019a,b), the oxygen fugacity of formation/alteration, and degree of aqueous alteration experienced (e.g., Schrader et al., 2021). The mean at.% Fe/S ratio of Ni-poor pyrrhotite in Tarda is 0.87, which indicates a high degree of oxidizing aqueous

alteration consistent with that seen in CI (Fe/S = 0.85–0.87) and CM1/2 (Fe/S = 0.89–0.91) chondrites by Schrader et al. (2021). Pyrrhotite-pentlandite geothermometry via phase diagram analysis (e.g., Schrader et al., 2016) shows Tarda sulfide equilibration temperatures of approximately 100–135°C (Fig. 9a), which is consistent with formation of the sulfides during low-temperature aqueous alteration, and provides an estimate for the minimum parent asteroid alteration temperature of Tarda. The sulfide equilibration temperature is not the peak metamorphic temperature a sample was exposed to, but are rather the temperature at which the sulfide minerals equilibrated. Therefore, the sulfide equilibration temperature provides a minimum temperature of alteration (Schrader et al., 2016). Following the work of Kimura et al. (2008), the low Co content of Ni-poor Fe,Ni metal (Table 4) is also consistent with Tarda being relatively unheated (i.e., similar to that of petrographic types 3.00 to <3.10). Therefore, assuming similar temperatures for 3.00 to <3.10 petrographic type chondrites (Busemann et al., 2007), the peak temperature our samples of Tarda were exposed to can be inferred to be ≲300°C. Our pyrrhotite-pentlandite geothermometry of Tagish Lake also shows sulfide equilibration temperatures of approximately 100–135°C (Fig. 9b), the same equilibration temperature as determined for sulfides in Tarda, indicating similar parent body alteration histories. These temperatures are similar to the aqueous alteration temperatures estimated for the CI chondrites (Bullock et al., 2005; Berger et al., 2011) and for the most altered CM chondrites (Schrader et al., 2016) from sulfide geothermometry.

4.1.4. Carbonate chemical compositions

The types and/or compositions of carbonates vary between distinct meteorite groups. For example, CI chondrites contain calcite/aragonite ($CaCO_3$), breunnerite ($[Mg,Fe]CO_3$), siderite ($FeCO_3$), and abundant dolomite ($CaMg[CO_3]_2$), while CM chondrites contain calcite/aragonite and dolomite (e.g., Fredricksson and Kerridge, 1988; Johnson and Prinz, 1993; Nakamura et al., 2003; de Leuw et al., 2010). In comparison, carbonates in CR chondrites are dominantly calcite, and while rare dolomite has been observed, no siderite has been reported (e.g., Weisberg et al., 1993; Weisberg and Huber, 2007; Schrader et al., 2014; Jilly-Rehak et al., 2018).

The carbonates in Tagish Lake are typically ferromagnesian (siderite and dolomite), although calcite is also present (Nakamura et al., 2003; Blinova et al., 2014). We analyzed carbonates in Tarda and Tagish Lake, as well as the CI chondrite Orgueil and the CM1/2 chondrite Kolang to investigate if the chemical compositions of carbonates are noticeably different between different

meteorite groups (Fig. 10; Table 5). We identified ferromagnesian carbonates in all samples, but calcite was only observed in Tagish Lake (C2-ung) and Kolang (CM1/2). We did not find calcite in Tarda, nor did Marrocchi et al. (2021). We find that Tarda dolomites are compositionally similar to those in CI and CM chondrites, but contain less FeO and MnO than those in Tagish Lake (Fig. 10). The CI Orgueil contains some dolomite grains with the lowest FeO and MnO contents and Tagish Lake dolomite grains contain higher FeO and MnO contents than the other samples studied here (Table 5; Fig. 10). In general, we did not identify clear compositional differences in dolomite between CI, CM1/2, and Tarda that could be used as a diagnostic indicator between them. Instead, the types of carbonate minerals present in a meteorite likely provide valuable information about the local alteration histories present in their parent asteroids.

Since Tarda and Tagish Lake likely originate from the same parent body, the difference in carbonate minerals present in Tarda (only dolomite) and Tagish Lake (dolomite, siderite, and rare calcite) may indicate differences in alteration histories/degrees of alteration within a single asteroid. The higher Fe and Mn content of dolomite in Tagish Lake than that of Tarda may also be an indicator of different alteration histories/fluid compositions. In terrestrial settings, dolomite can form (1) by replacement of Ca in calcite by Mg, or (2) from direct precipitation in clay minerals (e.g., Casado et al., 2014; Wanas and Sallam, 2016). The source of Mg in terrestrial dolomite is typically considered to be neighboring Mg-bearing clay minerals (e.g., Cai et al., 2021), perhaps suggesting that dolomite is an indicator of more extensive aqueous alteration in carbonaceous chondrites, although specific alteration conditions, fluid chemistry, and phyllosilicate compositions likely are important factors in the specific compositions of carbonate formation. Factors controlling the Fe and Mn contents of dolomite are related to the environment of dolomite formation (Cai et al., 2021). In studies of terrestrial dolomite, Fe^{2+} and Mn^{2+} replace Mg^{2+} in pre-existing dolomite (Cai et al., 2021). Therefore, the Fe- and Mn-enriched dolomite in Tagish Lake (compared to that in Tarda) may indicate a distinct degree or condition(s) of alteration. Since Tarda only contains dolomite, which is compositionally similar to dolomite in the CI and the CM1/2 chondrites, it may indicate that Tarda is more aqueously altered than Tagish Lake or that their specific conditions of aqueous alteration were different. Since Tarda and Tagish Lake contain similar phyllosilicate abundances (~86.9 and ~86.2 vol.%, respectively; Table 2) and H contents (Fig. 6a), it seems more likely that the two meteorites have experienced similar degrees of aqueous alteration but that their fluid compositions during aqueous alteration differed. This may indicate

605 evolving fluid compositions in an asteroid, similar to that proposed by Jilly-Rehak et al. (2018) for
606 CR chondrites.
607
608 *4.1.5. Chondrule sizes and olivine compositions*
609 Average chondrule diameters vary between different chondrite groups and have been used as
610 a parameter for meteorite classification (Weisberg et al., 2006; Jones, 2012). The apparent (2D)
611 mean chondrule diameter for Tarda (0.26±0.12 mm [2SE], n = 21) is most similar to that of Tagish
612 Lake (0.29±0.05 mm [2SE], n = 57; this study). Compared to known meteorite groups, Tarda's
613 apparent (2D) mean chondrule diameter is larger that of the CM chondrites (mean 0.17 mm; Mouti
614 Al-Hashimi et al., 2023) and the CO chondrites (mean 0.15 mm; Rubin, 1989). Our apparent (2D)
615 chondrule diameter range for Tagish Lake (0.05–1.37 mm) is similar to that reported by Zolensky
616 et al. (2002) and Blinova et al. (2014) (0.1–2 mm; mean diameters were not reported). Based on
617 the apparent (2D) mean chondrule diameters, the samples of Tarda and Tagish Lake studied here
618 are very similar.
619 The Fe-Mn systematics of chondrule olivines can help identify genetic relationships between
620 groups (e.g., Berlin et al., 2011; Schrader and Davidson, 2017; 2022; Schrader et al., 2020). The
621 Fe-Mn compositions of FeO-poor and FeO-rich chondrule olivines in Tarda are most similar to
622 those of chondrules in Tagish Lake (Figs. 11a,b), and CO and CM chondrites (Berlin et al., 2011;
623 Schrader and Davidson, 2017, 2022; Schrader et al., 2020). The *in situ* O isotope compositions of
624 FeO-poor chondrule olivines from Tarda are also similar to those of Tagish Lake (Ushikubo and
625 Kimura, 2021; Marrocchi et al., 2021), as well as CM and CO chondrites (e.g., Ushikubo and
626 Kimura, 2021). While the distinct bulk O isotope compositions (Gattacceca et al., 2021), H-C-N
627 compositions (Fig. 6 and Table 6), and Cr and Ti compositions (Fig. 7) exclude the possibility that
628 Tarda is a CM or CO chondrite, Tarda's chondrules may have formed under similar conditions
629 from similar precursor materials.
630
631 *4.1.6. Spectral comparison*
632 Tarda shows both spectral similarities and differences when compared to Tagish Lake (Figs.
633 12 and 13). Continuum-removed 350–2500 nm reflectance spectra of Tagish Lake show no strong
634 (>1% deep) absorption bands (Izawa et al., 2015). Continuum-removed 350–2500 nm spectra of
635 Tarda (Figs. 14a,b) in the ~1000 nm region reveal a possible weak absorption feature (<4% deep)

(Figs. 14c,d). In the Tarda powder spectra, well-resolved absorption features are present near 900 nm and 1100 nm, as well as a shoulder near 1400 nm. The 900 nm and 1100 nm bands are consistent with Fe^{2+}-bearing phyllosilicates (Clark et al., 1990), and share similarities with other aqueously-altered carbonaceous chondrites, such as CI and CM chondrites (e.g., Cloutis et al., 2011a,b). The 1400 nm shoulder is consistent with the presence of OH/H_2O (Clark et al., 1990). The chip spectrum shows weaker absorption features than the powder spectrum. However, the 900 nm, 1100 nm, and 1400 nm absorption features all appear to be present. There is also a relatively strong ~700 nm absorption feature that is attributable to an Fe^{3+}–Fe^{2+} charge transfer in the phyllosilicates (Clark et al., 1990; Cloutis et al., 2011b); this feature is also suggested in the powder spectrum as a shoulder or inflection point near this wavelength.

Mid-infrared reflectance spectra of numerous carbonaceous chondrites, including Tagish Lake, have been collected (Izawa et al., 2010; Vernazza et al., 2013; McAdam et al., 2015; Lantz et al., 2017; Beck et al., 2018; Morlok et al., 2020; Thompson et al., 2020; Hiroi et al., 2021; Poggiali et al., 2021). These spectra are largely dominated by the Si-O stretching reststrahlen bands (RBs) of phyllosilicates (at ~9.8 μm), olivine (multiple overlapping RBs near 9–11 μm), and pyroxene (multiple overlapping RBs near 9–11 μm) (Poggiali et al., 2021). Here, we show that the Si-O stretching region of Tarda most closely resembles that of Tagish Lake (Fig. 13), in comparison to other carbonaceous chondrites, consistent with the spectroscopic analysis by Yesiltas et al. (2022). The most prominent feature observed for Tarda is the phyllosilicate RB, observed strongly at ~9.80 μm for the chip spectrum and, as expected, more weakly for the fine-grained powder. Due to the low concentration of other silicates in Tagish Lake and Tarda (Izawa et al., 2010; this study, Table 2), the feature near 11.5 μm is not an RB, but rather a transparency feature (TF). This TF spectrally behaves differently, as expected, and is most prominent in the fine-grained sample spectra. Similar results and spectral appearances are qualitatively similar for the samples of Tagish Lake measured by Poggiali et al. (2021), and from the spectra in the RELAB database of Tagish Lake ET01-B (Fig. 15).

Of the known chondrite groups, the reflectance spectra of Tarda appear most like those of some of the CI chondrites in terms of low albedo, spectral shapes (slope), and lack of well-defined absorption bands below 2500 nm (e.g., Cloutis et al., 2011a), but without any strong matches. Overall, the VNIR spectral properties of Tarda are better matched by Tagish Lake, WIS 91600, and MET 00432 (Figs. 12a,b).

667

668 **4.2. Comparison to WIS 91600 and MET 00432: A new carbonaceous chondrite grouplet?**

669 WIS 91600 and MET 00432 have been suggested to be related to Tagish Lake, and have been
670 dubbed Tagish Lake-like meteorites (e.g., Alexander et al., 2007; Moriarty et al., 2009; Yabuta et
671 al., 2010; Yamanobe et al., 2018). The bulk O isotope composition of WIS 91600 ($\Delta^{17}O = -0.08‰$;
672 Clayton and Mayeda, 2003) is distinct from those of CM chondrites but very similar to that of
673 Tagish Lake (e.g., Fig. 2 in Moriarty et al., 2009) and Tarda (e.g., Gattacceca et al., 2021). The Cr
674 and Ti isotopic compositions of WIS 91600 are also very similar to Tarda and Tagish Lake (Fig.
675 7; Render et al., 2022; Hellman et al., 2023). WIS 91600 resembles some lithologies of Tagish
676 Lake on the basis of the similar elemental and $\delta^{15}N$ isotopic compositions of their macromolecular
677 organic matter, although they have distinct N/C ratios, δD and $\delta^{13}C$ isotopic compositions
678 (Alexander et al., 2007). In addition, based on siderophile/lithophile element ratios, Moriarty et al.
679 (2009) proposed that WIS 91600 is more closely related to the CM chondrites than it is to Tagish
680 Lake. The bulk elemental composition of WIS 91600 (Choe et al., 2010) is similar to the CM
681 chondrites (Fig. 8), as well as Tagish Lake (Brown et al., 2000) and Tarda (Figs. 8c,d). Based on
682 WIS 91600's distinct bulk O isotope composition and the H-C-N compositions of its
683 macromolecular organic matter compared to CM chondrites, we find it likely that it is not a CM
684 chondrite. Several studies indicate that WIS 91600 underwent mild shock heating <600°C (Yabuta
685 et al., 2010; Tonui et al., 2014; Hanna et al., 2020), which could complicate some of these
686 comparisons. Therefore, it is possible that (1) WIS 91600 shared the same parent body/asteroid as
687 Tagish Lake and Tarda, and that the bulk elemental composition of this asteroid is very similar to
688 that of the CM chondrites, (2) that WIS 91600 is related to the CM chondrites and not from the
689 same asteroid as Tagish Lake and Tarda, or (3) WIS 91600 shares similarities to but is from a
690 different parent asteroid than either the CM chondrites or Tagish Lake and Tarda.

691 While the bulk O isotope composition of MET 00432 is similar to that of Tagish Lake
692 (Yamanobe et al., 2018) and therefore Tarda, the bulk H, C, and N abundances and isotopic
693 compositions of MET 00432 are more similar to those of the CM chondrites (Alexander et al.,
694 2013), not Tagish Lake or Tarda. Since WIS 91600 and MET 00432 have numerous differences
695 from Tagish Lake and Tarda, they may not be from the same parent asteroid, or they may have
696 experienced distinct alteration histories. Based on the current data, we find it possible that all four
697 meteorites could be related, but more analyses are required to conclude if WIS 91600 and MET

00432 are from the same parent asteroid as Tarda and Tagish Lake. Primarily, apparent (2D) chondrule sizes, modal mineralogies, and chemical compositions of major minerals are needed. Correlated H, C, N, O, Cr, and Ti isotopes for WIS 91600 and MET 00432 could also help resolve this issue.

Tarda shows both spectral similarities and differences when compared to the Tagish Lake-like meteorites (Figs. 12 and 13). Detailed spectroscopic analysis is hampered by their low overall reflectance, which makes identification of subtle absorption bands somewhat uncertain. Spectral shapes in the 500–2500 nm region range from concave up (Tarda) to concave down (MET 00432) (Fig. 12). Spectral slopes, as measured by the 2500/555 nm reflectance ratio are all red, ranging from ~1.3 to ~1.7 (a red slope is defined as a spectrum with increasing reflectance toward longer wavelengths).

When compared with Tagish Lake and WIS 91600, the 350–2500 nm reflectance spectra of Tarda exhibits a less-red spectral slope (Fig. 12b). The spectral slope is closest to that of MET 00432, but spectral slopes are sensitive to grain size (Cloutis et al., 2011a,b). The overall albedo of Tarda is very similar to Tagish Lake and WIS 91600 (Fig. 12a), which may be expected, given the relatively similar concentration of opaque minerals (Table 2). The most noticeable difference between Tarda and the other Tagish Lake-like meteorites is the existence of the upward concave spectral shape. In addition, different lithologies of Tagish Lake show variations in both albedo and spectral slope (Fig. 15).

These results suggest that Tarda has strong similarities with the Tagish Lake-like meteorites, yet exhibits some spectral properties and within-grouplet differences that are similar to those seen in CI and CM chondrites (Cloutis et al., 2011a,b), as well as within different lithologies of Tagish Lake (Izawa et al., 2015; Fig. 15). It remains to be seen whether multiple lithologies are identified among samples of Tarda, although none were identified in this study or by Marrocchi et al. (2021). Based on the similarities between Tarda and Tagish Lake, the finding of distinct Tarda lithologies would not be surprising, given the spectral and compositional diversity in Tagish Lake lithologies (Izawa et al., 2015; Gilmour et al., 2019).

Through a comparison of the reflectance spectra of all carbonaceous chondrite groups and ungrouped samples (e.g., Cloutis et al. 1994, 2011a,b, 2012a,b,c,d,e,f; Donaldson Hanna et al., 2019), we find that the VNIR spectral properties of Tarda are better matches with Tagish Lake, WIS 91600, and MET 00432 than any other meteorite or known meteorite group (Figs. 12a,b). In

Figures 12a,b, we show Tarda compared to WIS 91600, MET 00432, and Tagish Lake as they are most similar in terms of albedo, spectral slope, and weak or non-existent absorption bands. These similarities support that Tarda, Tagish Lake, WIS 91600, and MET 00432 are potentially related or at least contain similar minerals.

4.3. The Tagish Lake-like meteorites and links to asteroids

4.3.1. P-type and D-type asteroids

P-type and D-type asteroids are both considered to be spectrally featureless in the ~0.4-2.5 μm region. Both groups are dark (geometric albedos ≲0.03) but are distinguished mainly in terms of their spectral slopes, with D-type asteroids having steeper red-sloped spectra than P-type asteroids (Tholen, 1984). Multiple explanations have been advanced to explain this, mainly textural and compositional.

Vilas and Smith (1985) studied the ~0.5–1.0 μm region reflectance spectra of a number of P- and D-type asteroids. They found that the D-type asteroids have broadband reflectance spectra which are low in the UV-visible spectral region, and exhibit an increase in relative reflectance beginning around 0.7 μm. They also have low geometric albedos (~0.03) as derived from thermal radiometry (10- and 20-μm observations). The broadband spectra of some D-type asteroids flatten in the near-infrared, while other spectra increase linearly in this interval. The P-type asteroids have linear spectra showing a slight increase in slope with increasing wavelength, and low albedos (~0.03) comparable to the D-type asteroids. From this information, they subdivided the spectra into four subgroups on the basis of spectral slope: two P-subgroups with flat barely-sloping spectra or small positive slopes, and two D-subgroups with different red slopes. They provided two possible explanations related to hydrocarbons: (1) simpler hydrocarbons with increasing heliocentric distance or (2) color changes in hydrocarbons with increasing heliocentric distance (i.e., temperature).

Fitzsimmons et al. (1994) found a possible correlation between asteroid diameter and color (spectral slope). They speculated that this was due to redder objects being inherently weaker and less resistant to break-up following impacts or, alternatively, that variations in shock processes during collisions. Barucci et al. (1987) and Fitzsimmons et al. (1994) found spectral variations

759 within the D-type in terms of spectral shape, between concave and convex, and derived four
760 subgroups using slope and shape criteria.
761 Analysis of P-type asteroids in terms of carbonaceous chondrite spectra indicated that P-type
762 asteroids spectra can be reproduced by different proportions of various carbonaceous chondrites,
763 suggesting that compositional differences may explain the spectral differences between P- and D-
764 type asteroids (Hiroi et al., 2004).
765
766 *4.3.2. A genetic relationship between P- and D-type asteroids*
767 Previous work has shown that some P-type asteroids exhibit reflectance spectra that can be
768 described as intermediate between CI/CM chondrites and Tagish Lake (Hiroi et al., 2004). Given
769 the strong spectral similarities of Tarda to the Tagish Lake-like meteorites, albeit with subtle
770 similarities to some CI spectra, Tarda could be described as a meteorite that falls within this
771 intermediate space.
772 The VNIR spectral shape of Tarda does not closely match the mean values found for D-type
773 asteroids presented by DeMeo et al. (2009) (Fig. 16). Tarda is less red-sloped and shows variations
774 in spectral slope over the 400–2500 nm interval as compared to D-type asteroids. Instead, the
775 spectral slope and shape of the Tarda meteorite spectra share affinities with some Tholen (Tholen,
776 1989) taxonomic P-type and/or Bus X/Xc-type asteroids (Bus and Binzel, 2002a), with a
777 moderately-red spectral slope, a slope break near 500 nm and no resolvable absorption band
778 between 400 nm and 500 nm (e.g., DeMeo et al., 2009) (Fig. 17). The reflectance spectra from
779 both P-type asteroids 65 Cybele and 76 Freia (Bus and Binzel, 2002b; Burbine and Binzel, 2002;
780 Rayner et al., 2003) fall between the spectral slopes of the Tarda powder and chip, which may
781 suggest variations in the grain size distribution of Tholen P-type asteroid surfaces (e.g.,
782 Fitzsimmons et al., 1994). The visible spectral shapes of these two asteroids also resemble that
783 exhibited by Tarda. Given the similarities in spectral slope and visible spectral shape, it is likely
784 that Tarda and these asteroid surfaces are made of similar materials.
785 The petrologic, chemical, and isotopic characteristics of Tarda and Tagish Lake (§4.1) are
786 similar enough that there is a strong possibility that Tarda originated from the same outer Solar
787 System asteroid as Tagish Lake. If they are not from the same asteroid, they at least formed from
788 similar precursor materials under similar conditions. Here, we find that the spectral reflectance
789 properties of Tarda most closely resemble those of the Tagish Lake-like meteorites, yet also

exhibits affinities with some CI/CM chondrites, such as low albedo, and spectral slope (like CI chondrites) and 1 μm region absorption features (like CM chondrites). The reflectance spectra from the lithology of Tarda analyzed here appear to be a closer match to some Tholen P-type asteroids than to Tholen D-types. Should additional samples of Tarda exhibit similar reflectance properties (to test if Tarda is as homogenous as we found here), it may be that Tarda could represent the first sample of a P-type asteroid surface. These results are not contradictory, but highlight that numerous other possible scenarios exist; including that very subtle compositional differences could explain variations in the spectral taxonomies of asteroids.

Since Tarda and Tagish Lake likely originated from the same parent asteroid, P-type and D-type asteroid types may be genetically related, and differ spectrally due to differences in grain size or small mineralogical variations. These variations could be due to the parent asteroid being heterogeneous or having distinct degrees of alteration. Alternately, P-type and D-type asteroids may now be separate objects, but may represent fragments of the same original parent asteroid. This highlights that these subtle compositional and/or grain size differences also affect meteorite reflectance spectra and that isolating the controlling variables of materials bearing multiple opaque phases with variations in chemical compositions is complex.

5. Conclusions and Implications

1) Comparable mineral chemistries, modal abundances, bulk elemental compositions, as well as abundances and isotopic compositions of H, C, N, Cr and Ti show that Tarda and Tagish Lake share a close genetic relationship, indicating that they originate from the same outer Solar System asteroid.

2) The Tarda meteorite shows several spectral similarities to other Tagish Lake-like meteorites; low visible region reflectance, an overall red spectral slope over the 350 to 2500 nm interval, and weak to non-existent absorption bands associated with their known mineralogies. The overall spectral shape of Tarda shows greater affinities for taxonomic P-type versus D-type asteroids (Tholen, 1989). Similarities in reflectance spectra suggest that P-type asteroids 65 Cybele and 76 Freia are potential parent bodies of Tarda and the Tagish Lake-like meteorites, or at least have similar surface materials.

3) Tarda is a closer spectral match to a P-type asteroid (this study) and Tagish Lake is a closer spectral match to a D-type asteroid (Hiroi et al., 2005). Since Tarda and Tagish Lake likely originated from the same parent asteroid, P-type and D-type asteroid types may be genetically related, and differ spectrally due to differences in grain size or small mineralogical variations. This spectral difference among related samples is evidenced by the fact that subsamples of Tagish Lake show variations in spectral slope due to compositional variations. While different grain size fractions of a single lithology of Tagish Lake have not been spectrally characterized, other carbonaceous chondrite powders show differences in spectral slope due to grain size variations (Cloutis et al., 2018). Alternately, P-type and D-type asteroids may now be separate objects, but may represent fragments of the same original parent asteroid.

4) Tarda is a highly hydrated type 2 carbonaceous chondrite that will likely provide an informative comparison to the heavily hydrated CI-like material returned by Hayabusa2 from C-type asteroid Ryugu (e.g., Yokoyama et al., 2022) and the material returned by OSIRIS-REx from B-type asteroid Bennu (e.g., Hamilton et al., 2019) on September 24th, 2023. Additionally, because of the potential relationship between P-type and D-type asteroids, Tarda is particularly important to study in preparation for and comparison to the spectra of D-type (11351 Leucus and 21900 Orus) and P-type (15094 Polymele, and 617 Patroclus and its binary companion Menoetius) Trojan asteroids to be surveyed by NASA's Lucy mission (e.g., Levison et al., 2021), and spectra of and samples from Mars' moon Phobos (similar to D-type asteroids) to be returned by JAXA's MMX mission (Nakamura et al., 2021; Kuramoto et al., 2022).

Acknowledgments: We thank the ASU Buseck Center for Meteorite Studies for providing Tarda and Tagish Lake from the Carleton B. Moore meteorite collection and the Smithsonian Institution and NASA/NSF for the sample of MET 00432. We also thank Laurence Garvie for preparing polished mounts of Tarda and Tagish Lake. US Antarctic meteorite samples are recovered by the Antarctic Search for Meteorites (ANSMET) program, which has been funded by NSF and NASA, and characterized and curated by the Department of Mineral Sciences of the Smithsonian Institution and Astromaterials Acquisition and Curation Office at NASA Johnson Space Center. We are grateful to Axel Wittmann for assistance with the EPMA at ASU. We thank Prof. Sho Sasaki for providing us the opportunity to use a spectrometer at Mizusawa Very Long Baseline Interferometer (VLBI) Observatory. We are also grateful to Yves Marrocchi, two anonymous reviewers, and Associate Editor Frederic Moynier, whose constructive comments improved the quality of the manuscript. This study was supported by NASA grants NNX17AE53G (DLS PI, TJZ Co-I) and 80NSSC19K0559, 80NSSC20K0344, 80NSSC21K0654 (DF, CA), an ASU Investigator Incentive Award (DLS), the Canadian Space Agency (CSA; grant 22EXPOSIWI), the Natural Sciences and Engineering Research Council of Canada (NSERC grants RTI-2020-00157, and RTI-2018-0032), the University of Winnipeg, and a Carnegie Postdoctoral Fellowship (ZAT). Portions of this study were performed under the auspices of the US DOE by Lawrence Livermore National Laboratory under Contract DE-AC52-07NA27344 with release number LLNL-JRNL-853504. The Centre for Terrestrial and Planetary Exploration (C-TAPE; https://www.uwinnipeg.ca/c-tape/index.html) was established with funding from the Canada Foundation for Innovation (CFI, grant #1504 and 245), the Manitoba Research Innovations Fund, and the CSA. Part of the data utilized in this publication were obtained and made available by the MITHNEOS MIT-Hawaii Near-Earth Object Spectroscopic Survey. The IRTF is operated by the University of Hawaii under contract 80HQTR19D0030 with the National Aeronautics and Space Administration. The MIT component of this work is supported by NASA grant 80NSSC18K0849. Any opinions, findings, and conclusions or recommendations expressed in this material are those of the author(s) and do not necessarily reflect the views of NASA or the National Science Foundation. We acknowledge the use of facilities within the Eyring Materials Center at Arizona State University supported in part by NNCI-ECCS-1542160.

APPENDIX A. SUPPLEMENTARY MATERIAL

Supplementary Material (SM) consist of four files. These files contain: (SM 1) all images and X-ray maps of samples, with the location of electron microprobe analyses: (SM 2) chondrule size measurements for Tarda and Tagish Lake; (SM 3) all electron microprobe data; and (SM 4) reflectance spectra.

Data Availability

Data are available through Mendeley Data at https://doi.org/10.17632/2s8hvm3df2.1.

887 **REFERENCES**

888

889 Adler, H. H. and Kerr, P. F. (1963a) Infrared absorption frequency trends for anhydrous normal
890 carbonates. *Am. Mineral.* **48**, 124–137.
891 Adler, H. H. and Kerr, P. F. (1963b) Infrared spectra, symmetry and structure relations of some
892 carbonate minerals. *Am. Mineral.* **48**, 839–853.
893 Alexander C.M.O'D., Fogel M., Yabuta H., and Cody G. D. (2007) The origin and evolution of
894 chondrites recorded in the elemental and isotopic compositions of their macromolecular
895 organic matter. *Geochim. Cosmochim. Acta* **71**, 4380–4403.
896 Alexander C. M. O. D., Newsome S. D., Fogel M. L., Nittler L. R., Busemann H., and Cody G. D.
897 (2010) Deuterium enrichments in chondritic macromolecular material-Implications for the
898 origin and evolution of organics, water and asteroids. *Geochim. Cosmochim. Acta* **74**, 4417–
899 4437.
900 Alexander C. M. O'D., Bowden R., Fogel M. L., Howard K. T., Herd C. D. K., and Nittler L. R.
901 (2012) The provenances of asteroids, and their contributions to the volatile inventories of the
902 terrestrial planets. *Science* **337**, 721–723.
903 Alexander C. M. O'D., Howard K. T., Bowden R., and Fogel M. L. (2013) The classification of
904 CM and CR chondrites using bulk H, C and N abundances and isotopic compositions.
905 *Geochim. Cosmochim. Acta* **123**, 244–260.
906 Alexander C. M. O'D., Greenwood R. C., Bowden R., Gibson J. M., Howard K. T., and Franchi
907 I. A. (2018) A multi-technique search for the most primitive CO chondrites. *Geochim.*
908 *Cosmochim. Acta* **221**, 406–420.
909 Avice G., Meier M. M. M., and Marrocchi Y. (2022) Origin of radiogenic ^{129}Xe variations in
910 carbonaceous chondrites. *Geochem. Persp. Let.* **23**, 1–4.
911 Barucci, M.A., M.T. Capria, A. Coradini, and M. Fluchignoni (1987) Classification of asteroids
912 using G-mode analysis. *Icarus* **72**, 304–324.
913 Beck P., Maturilli A., Garenne A., Vernazza P., Helbert J., Quirico E., and Schmitt B. (2018).
914 What is controlling the reflectance spectra (0.35–150 μm) of hydrated (and dehydrated)
915 carbonaceous chondrites? *Icarus* **313**, 124–138.
916 Bellamy, L.J. (1958) The Infra-red Spectra of Complex Organic Molecules, 2nd ed. John Wiley
917 and Sons Inc., New York.
918 Berger E. L., Zega T. J., Keller L. P. and Lauretta D. S. (2011) Evidence for aqueous activity on
919 comet 81P/Wild 2 from sulfide mineral assemblages in Stardust samples and CI chondrites.
920 *Geochim. Cosmochim. Acta* **75**, 3501–3513.
921 Berlin J., Jones R. H., and Brearley A. J. (2011) Fe-Mn systematics of type IIA chondrules in
922 unequilibrated CO, CR, and ordinary chondrites. *Meteorit. Planet. Sci.* **46**, 513–533.
923 Blinova A. I., Zega T. J., Herd C. D. K., and Stroud R. M. (2014) Testing variations within the
924 Tagish Lake meteorite—I: Mineralogy and petrology of pristine samples. *Meteorit. Planet.*
925 *Sci.* **49**, 473–502.
926 Brown P. G., Hildebrand A. R., Zolensky M. E., Grady M., Clayton R. N., Mayeda T. K.,
927 Tagliaferri E., Spalding R., Macrae N. D., Hoffman E. L., Mittlefehldt D. W., Wacker J. F.,
928 Bird A., Campbell M. D., Carpenter R., Gingerich H., Glatiotis M., Greiner E., Mazur M. J.,
929 McCausland P. JA., Plotkin H., and Rubak Mazur T. (2000) The Fall, Recovery, Orbit, and
930 Composition of the Tagish Lake Meteorite: A New Type of Carbonaceous Chondrite. *Science*
931 **290**, 320–325.

Bryson J. F. J., Weiss B. P., Biersteker J. B., King A. J., and Russell S. S. (2020) Constraints on the Distances and Timescales of Solid Migration in the Early Solar System from Meteorite Magnetism. *Astrophys. J.* **892**, 126.

Burbine T. H. and Binzel R. P. (2002) Small Main-Belt Asteroid Spectroscopic Survey in the Infrared. *Icarus* **159**, 468–499.

Bus S. J., and Binzel R. P. (2002a) Phase II of the Small Main-Belt Asteroid Spectroscopic Survey: A Feature-Based Taxonomy. *Icarus* **158**, 146–177.

Bus S. J. and Binzel R. P. (2002b) Phase II of the Small Main-Belt Asteroid Spectroscopic Survey: The Observations. *Icarus* **158**, 106–145.

Busemann H., Alexander C. M. O'D. and Nittler L. R. (2007) Characterization of insoluble organic matter in primitive meteorites by microRaman spectroscopy. *Meteorit. Planet. Sci.* **42**, 1387–1416.

Cai W. K., Liu J. H., Zhou C. H., Keeling J., and Glasmacher U. A. (2021) Structure, genesis and resources efficiency of dolomite: New insights and remaining enigmas. *Chem. Geol.* **573**, 120191.

Casado A. I., Alonso-Zarza A. M., La Iglesia Á. (2014) Morphology and origin of dolomite in paleosols and lacustrine sequences. Examples from the Miocene of the Madrid Basin. *Sediment. Geol.* **312**, 50–62.

Choe W. H., Huber H., Rubin A. E., Kallemeyn G. W., and Wasson J. T. (2010) Compositions and taxonomy of 15 unusual carbonaceous chondrites. *Meteorit. Planet. Sci.* **45**, 531–554.

Clark R. N., King T. V. V., Klewja M., Swayze G. A., and Vergo N. (1990) High spectral resolution reflectance spectroscopy of minerals. *J. Geophys. Res.* **95**, 12,653–12,680.

Clayton R. N. and Mayeda T. K. (1999) Oxygen isotope studies of carbonaceous chondrites. *Geochim. Cosmochim. Acta* **63**, 2089–2104.

Clayton R. N. and Mayeda T. K. (2003) Oxygen isotopes in carbonaceous chondrites. In Evolution of solar system materials: A new perspective from Antarctic meteorites. Tokyo: NIPR. pp. 13–14.

Cloutis E. A., Gaffey M. J., and Moslow T. F. (1994) Spectral reflectance properties of carbon-bearing materials. *Icarus* **107***,* 276–287.

Cloutis E. A., Hiroi T., Gaffey M. J., Alexander C. M.O'D., and Mann P. (2011a) Spectral reflectance properties of carbonaceous chondrites: 1. CI chondrites. *Icarus* **212**, 180–209.

Cloutis E. A., Hudon P., Hiroi T., Gaffey M. J., and Mann P. (2011b) Spectral reflectance properties of carbonaceous chondrites: 2. CM chondrites. *Icarus* **216***,* 309–346.

Cloutis, E.A., Hudon P., Hiroi T., and Gaffey M. J. (2012a) Spectral reflectance properties of carbonaceous chondrites 4: Aqueously altered and thermally metamorphosed meteorites. *Icarus* **220**, 586-617.

Cloutis E. A., Hudon P., Hiroi T., and Gaffey M. J. (2012b) Spectral reflectance properties of carbonaceous chondrites: 3. CR chondrites. *Icarus* **217**, 389–407.

Cloutis E. A., Hudon P., Hiroi T., Gaffey M. J., and Mann P. (2012c) Spectral reflectance properties of carbonaceous chondrites: 5. CO chondrites. *Icarus* **220**, 466–486.

Cloutis E. A., Hudon P., Hiroi T., Gaffey M. J., Mann P., and Bell III J. F. (2012d) Spectral reflectance properties of carbonaceous chondrites: 6. CV chondrites. *Icarus* **221**, 328–358.

Cloutis E. A., Hudon P., Hiroi T., and Gaffey M. J. (2012e) Spectral reflectance properties of carbonaceous chondrites: 7. CK chondrites. *Icarus* **221**, 911–924.

Cloutis E. A., Hudon P., Hiroi T., Gaffey M. J., and Mann P. (2012f) Spectral reflectance properties of carbonaceous chondrites: 8. ‘‘Other’’ carbonaceous chondrites: CH, ungrouped, polymict, xenolithic inclusions, and R chondrites. *Icarus* **221**, 984–1001.

Cloutis E. A., Pietrasz V. B., Kiddell C., Izawa M. R. M., Vernazza P., Burbine T. H., DeMeo F., Tait K. T., Bell III J. F., Mann P., Applin D. M., and Reddy V. (2018) Spectral reflectance “deconstruction” of the Murchison CM2 carbonaceous chondrite and implications for spectroscopic investigations of dark asteroids. *Icarus* **305**, 203-224.

Davidson J., Schrader D. L., Busemann H., Franchi I. A., Connolly, Jr., H. C., Lauretta D. S., Alexander C. M. O’D., Verchovsky A. and Greenwood R. C. (2014) Petrography, stable isotope compositions, microRaman spectroscopy and presolar components of Roberts Massif 04133: A reduced CV3 carbonaceous chondrite. *Meteorit. Planet. Sci.* **49**, 2133–2151.

Davidson J., Alexander C. M. O’D., Stroud R. M., Busemann H. and Nittler L. R. (2019a) Mineralogy and petrology of Dominion Range 08006: A very primitive CO3 carbonaceous chondrite. *Geochim. Cosmochim. Acta* **265**, 259–278.

Davidson J., Schrader D. L., Alexander C. M. O’D., Nittler L. R. and Bowden R. (2019b) Re-examining thermal metamorphism of the Renazzo-like (CR) carbonaceous chondrites: Insights from pristine Miller Range 090657 and shock-heated Graves Nunataks 06100. *Geochim. Cosmochim. Acta* **267**, 240–256.

de Leuw S., Rubin A. E., and Wasson J. T. (2010) Carbonates in CM chondrites: Complex formational histories and comparison to carbonates in CI chondrites. *Meteorit. Planet. Sci.* **45**, 513–530.

DeMeo F. E., Binzel R.P., Slivan S. M., and Bus S. J. (2009) An extension of the Bus asteroid taxonomy into the near-infrared. *Icarus* **202**, 160–180.

Donaldson Hanna K. L., Schrader D. L., Cloutis E. A., Cody G. D., King A. J., McCoy T. J., Applin D. M., Mann J. P., Bowles N. E., Brucato J. R., Connolly H. C. Jr., Dotto E., Keller L. P., Lim L. F., Clark B. E., Hamilton V. E., Lantz C., Lauretta D. S., Russell S. S., and Schofield P. F. (2019) Spectral Characterization of Analog Samples in Anticipation of OSIRIS-REx’s Arrival at Bennu: A Blind Test Study. *Icarus* **319**, 701–723.

Eisenhour D. D. (1996) Determining chondrule size distributions from thin-section measurements. *Meteorit. Planet. Sci.* **31**, 243–248.

Fitzsimmons A., Dahlgren M., Lagerkvist C.-I., Magnusson P., and Williams I. P. (1994) A spectroscopic survy of D-type asteroids. *Astron. Astrophys.* **282**, 634–642.

Fredricksson K. and Kerridge J. F. (1988) Carbonates and sulfates in CI chondrites: Formation by aqueous activity on the parent body. *Meteoritics* **23**, 35–44.

Friedrich J. M., Wang M-S., and Lipschutz M. E. (2002) Comparison of the trace element composition of Tagish Lake with other primitive carbonaceous chondrites. *Meteorit. Planet. Sci.* **37**, 677–686.

Foustoukos D. I., Alexander C.M.O.D. and Cody G. D. (2021) H and N systematics in thermally altered chondritic insoluble organic matter: An experimental study. *Geochim. Cosmochim. Acta* **300**, 44–64.

Gaffey S. J. (1986) Spectral reflectance of carbonate minerals in the visible and near infrared (0.35-2.55 microns): calcite, aragonite, and dolomite. *Am. Mineral.* 71, 151–162.

Garvie L. A. J., Trif L., Cotto-Figueroa D., Asphaug E., and Hoover C. G. (2024) High surface area and interconnected nanoporosity of clay-rich astromaterials. *Scientific Reports* **14**, 10358.

Gattacceca J., McCubbin F. M., Grossman J., Bouvier A., Bullock E., Chennaoui Aoudjehane H., Debaille V., D'Orazio M., Komatsu M., Miao B., and Schrader D. L. (2021) The Meteoritical Bulletin, No. 109. *Meteorit. Planet. Sci.* **56**, 1626–1630.

Gerber S., Burkhardt C., Budde G., Metzler K., and Kleine T. (2017) Mixing and Transport of Dust in the Early Solar Nebula as Inferred from Titanium Isotope Variations among Chondrules. *Astrophys. J. Lett.* **841**, L17.

Gilmour C. M., Herd C. D., and Beck, P. (2019). Water abundance in the Tagish Lake meteorite from TGA and IR spectroscopy: Evaluation of aqueous alteration. *Meteorit. Planet. Sci.* **54**, 1951–1972.

Göpel C., Birck J-L., Galy A., Barrat J-A., and Zanda B. (2015) Mn–Cr systematics in primitive meteorites: Insights from mineral separation and partial dissolution. *Geochim. Cosmochim. Acta* **156**, 1–24.

Greenberger R. N., Mustard J. F., Cloutis E. A., Pratt L. M., Sauer P.E., Mann P., Turner K., Dyar M. D., and Bish D. L. (2015) Serpentinization, iron oxidation, and aqueous conditions in an ophiolite: Implications for hydrogen production and habitability on Mars. *Earth Planet. Sci. Lett.* **416***,* 21–34.

Greenwood R. C. and Franchi I. A. (2004) Alteration and metamorphism of CO3 chondrites: Evidence from oxygen and carbon isotopes. *Meteorit. Planet. Sci.* **39**, 1823–1838.

Greenwood R. C., Franchi I. A., Kearsley A. T. and Alard O. (2010) The relationship between CK and CV chondrites. *Geochim. Cosmochim. Acta* **74**, 1684–1705.

Grossman J. N. (2000) The Meteoritical Bulletin, No. 84, 2000 August. *Meteorit. Planet. Sci.* **35**, A199–A225.

Hamilton V., Simon A., Christensen P., Reuter D., Clark B., Barucci A., Bowles N., Boynton W., Brucato J., Cloutis E., Connolly Jr. H., Donaldson Hanna K., Emery J., Enos H., Fornasier S., Haberle C., Hanna R., Howell E., Kaplan H., Keller L., Lantz C., Li J.-Y., Lim L., McCoy T., Merlin F., Nolan M., Praet A., Rozitis B., Sandford S., Schrader D. L., Thomas C., Zou X.-D., Lauretta D., and the OSIRIS-REx Team. (2019) Evidence for widespread hydrated minerals on asteroid (101955) Bennu. *Nature Astronomy* **3**, 332–340.

Hanna R. D., Hamilton V. E., Haberle C. W., King A. J., Abreu N. M., and Friedrich J. M. (2020) Distinguishing relative aqueous alteration and heating among CM chondrites with IR spectroscopy. *Icarus* **346**, 113760.

Hellmann J. L., Schneider J. M., Wölfer E., Drążkowska J., Jansen C. A., Hopp T., Burkhardt C. and Kleine T. (2023) Origin of isotopic diversity among carbonaceous chondrites. *Astrophysical Journal Letters* **946**, L34.

Hewins R. H., Bourot-Denise M., Zanda B., Leroux H., Barrat J.-A., Humayun M., Gopël C., Greenwood R. C., Franchi I. A., Pont S., Lorand J.-P., Cournède C., Gattacceca J., Rochette P., Kuga M., Marrocchi Y. and Marty B. (2014) The Paris meteorite, the least altered CM chondrite so far. *Geochim. Cosmochim. Acta* **124**, 190–222.

Hibiya Y., Archer G. J., Tanaka R., Sanborn M. E., Sata Y., Iizuka T., Ozawa K., Walker R. J., Yamaguchi A., Yin Q-Z., Nakamura T., and Irving A. J. (2019) The origin of the unique achondrite Northwest Africa 6704: Constraints from petrology, chemistry and Re–Os, O and Ti isotope systematics. *Geochim. Cosmochim. Acta* **245**, 597–627.

Hiroi T., Zolensky M. E., and Pieters C. M. (2001) The Tagish Lake meteorite: A possible sample from a D-type asteroid. *Science* **293**, 2234–2236.

Hiroi T., Pieters C. M., Rutherford M. J., Zolensky M. E., Sasaki S., Ueda Y., and Miyamoto M. (2004) What are the P-type asteroids made of? *Lunar and Planetary Science Conference* XXXV, #1616 (abstract).

Hiroi T., Tonui E., Pieters C. M., Zolensky M. E., Ueda Y., Miyamoto M., and Sasaki S. (2005) Meteorite WIS91600: A new sample related to a D- or T-type asteroid. *Lunar and Planetary Science Conference* XXXVI, #1564 (abstract).

Hiroi T., Kaiden H., Imae N., Misawa K., Kojima H., Sasaki S., Matsuoka M., Nakamura T., Bish D. L., Ohtsuka K., Howard K. T., Robertson K. R., and Milliken R. E. (2021) UV-visible-infrared spectral survey of Antarctic carbonaceous chondrite chips. *Polar Sci.* **29**, 100723.

Hopp T., Dauphas N., Abe Y., Aléon J., Alexander C. M. O'D., Amari S., Amelin Y., Bajo K., Bizzarro M., Bouvier A., Carlson R. W., Chaussidon M., Choi B-G., Davis A. M., Di Rocco T., Fujiya W., Fukai R., Gautam I., Haba M. K., Hibiya Y., Hidaka H., Homma H., Hoppe P., Huss G. R., Ichida K., Iizuka T., Ireland T. R., Ishikawa A., Ito M., Itoh S., Kawasaki N., Kita N. T., Kitajima K., Kleine T., Komatani S., Krot A. N., Liu M-C., Masuda Y., McKeegan K. D., Morita M., Motomura K., Moynier F., Nakai I., Nagashima K., Nesvorný D., Nguyen A., Nittler L., Onose M., Pack A., Park C., Piani L., Qin L., Russell S. S., Sakamoto N., Schönbächler M., Tafla L., Tang H., Terada K., Terada Y., Usui T., Wada S., Wadhwa M., Walker R. J., Yamashita K., Yin Q-Z., Yokoyama T., Yoneda S., Young E. D., Yui H., Zhang A-C., Nakamura T., Naraoka H., Noguchi T., Okazaki R., Sakamoto K., Yabuta H., Abe M., Miyazaki A., Nakato A., Nishimura M., Okada T., Yada T., Yogata K., Nakazawa S., Saiki T., Tanaka S., Terui F., Tsuda Y., Watanabe S., Yoshikawa M., Tachibana S., and Yurimoto H. (2022) Ryugu's nucleosynthetic heritage from the outskirts of the Solar System. *Science Advances* **8**, eadd8141.

Izawa, M. R., Flemming, R. L., King, P. L., Peterson, R. C., & McCausland, P. J. (2010). Mineralogical and spectroscopic investigation of the Tagish Lake carbonaceous chondrite by X-ray diffraction and infrared reflectance spectroscopy. *Meteorit. Planet. Sci.* **45**, 675–698.

Izawa, M.R.M., M.A. Craig, D.M. Applin, J.A. Sanchez, V. Reddy, L. Le Corre, P. Mann, and E.A. Cloutis (2015) Variability, absorption features, and parent body searches in "spectrally featureless" meteorite reflectance spectra: Case study – Tagish Lake. *Icarus* **254***,* 324–332.

Jacquet E., Barrat J.-A., Beck P., Caste F., Gattacceca J., Sonzogni C. and Gounelle M. (2016) Northwest Africa 5958: A weakly altered CM-related ungrouped chondrite, not a CI3. *Meteorit. Planet. Sci.* **51**, 851–869.

Jamsja N. and Ruzicka A. (2010) Shock and thermal history of Northwest Africa 4859, an annealed impact-melt breccia of LL chondrite parentage containing unusual igneous features and pentlandite. *Meteorit. Planet. Sci.* **45**, 828–849.

Johnson C. A. and Prinz M. (1993) Carbonate compositions in CM and CI chondrites and implications for aqueous alteration. *Geochim. Cosmochim. Acta* **57**, 2843–2852.

Jones R. H. (1990) Petrology and mineralogy of type II, FeO-rich chondrules in Semarkona (LL3.0): Origin by closed-system fractional crystallization, with evidence for supercooling. *Geochim. Cosmochim. Acta* **54**, 1785–1802.

Jones R. H. (1992) On the relationship between isolated and chondrule olivine grains in the carbonaceous chondrite ALHA77307. *Geochim. Cosmochim. Acta* **56**, 467–482.

Jones R. H. (2012) Petrographic constraints on the diversity of chondrule reservoirs in the protoplanetary disk. *Meteorit. Planet. Sci.* **47**, 1176–1190.

Kadlag Y., Becker H., and Harbott A. (2019) Cr isotopes in physically separated components of the Allende CV3 and Murchison CM2 chondrites: Implications for isotopic heterogeneity in the solar nebula and parent body processes. *Meteorit. Planet. Sci.* **54**, 2116–2131.

Kimura K., Grossman J. N., and Weisberg M. K. (2008) Fe-Ni metal in primitive chondrites: Indicators of classification and metamorphic conditions for ordinary and CO chondrites. *Meteorit. Planet. Sci.* **43**, 1161–1177.

Kuramoto K., Kawakatsu Y., Fujimoto M., Araya A., Barucci M. A., Genda H., Hirata N., Ikeda H., Imamura T., Helbert J., Kameda S., Kobayashi M., Kusano H., Lawrence D. J., Matsumoto K., Michel P., Miyamoto H., Morota T., Nakagawa H., Nakamura T., Ogawa K., Otake H., Ozaki M., Russell S., Sasaki S., Sawada H., Senshu H., Tachibana S., Terada N., Ulamec S., Usui T., Wada K., Watanabe S., and Yokota S. (2022) Martian Moons Exploration MMX: Sample Return Mission to Phobos Elucidating Formation Processes of Habitable Planets. *Earth, Planets and Space* **74**, 1–31.

Lantz C., Brunetto R., Barucci M. A., Fornasier S., Baklouti D., Bourcois J., and Dodard M. (2017) Ion irradiation of carbonaceous chondrites: A new view on space weathering on primitive asteroids. *Icarus* **285**, 43-57.

Lee M. R., Hallis L. J., Daly L., and Boyce A. J. (2023) The water content of CM carbonaceous chondrite falls and finds, and their susceptibility to terrestrial contamination. *Meteorit. Planet. Sci.* **58**, 1760–1772.

Levison H. F., Olkin C. B., Noll K. S., Marchi S., Bell III J. F., Bierhaus E., Binzel R., Bottke W., Britt D., Brown M., Buie M., Christensen P., Emery J., Grundy W., Hamilton V. E., Howett C., Mottola S., Pätzold M., Reuter D., Spencer J., Statler T. S., Stern S. A., Sunshine J., Weaver H., and Wong I. (2021) Lucy Mission to the Trojan Asteroids: Science Goals. *Planetary Science Journal* **2**, 171.

Lodders K. (2021) Relative atomic Solar System Abundances, mass fractions, and atomic masses of the elements and their isotopes, composition of the solar photosphere, and compositions of the major chondritic meteorite groups. *Space Science Reviews* **217**, 44.

Marrocchi Y., Avice G., and Barrat J-A. (2021) The Tarda Meteorite: A Window into the Formation of D-type Asteroids. *Astrophys. J. Lett.* **913**, L9.

Marrocchi Y., Rigaudier T., Pirala M., and Piani L. (2023) Hydrogen isotopic evidence for nebular pre-hydration and the limited role of parent-body processes in CM chondrites. *Earth Planet. Sci. Lett.* **611**, 118151.

Metzler K. (2018) From 2D to 3D chondrule sizes: Some empirical ground truths. *Meteorit. Planet. Sci.* **53**, 1489–1499.

Metzler K., Hezel D. C., and Nellesen J. (2019) Various size-sorting processes for millimeter-sized particles in the Sun′s protoplanetary disk? Evidence from chondrules in ordinary chondrites. *Astrophys. J.* **887**, 230.

Metzler K., Hezel D. C., Barosch J., Wölfer E., Schneider J. M., Hellmann J. L., Berndt J., Stracke A., Gattacceca J., Greenwood R. C., Franchi I. A., Burkhardt C., and Kleine T. 2021. The Loongana (CL) group of carbonaceous chondrites. *Geochim. Cosmochim. Acta* **304**, 1–31.

McAdam M. M., Sunshine J. M., Howard K. T., and McCoy, T. M. (2015). Aqueous alteration on asteroids: Linking the mineralogy and spectroscopy of CM and CI chondrites. *Icarus* **245**, 320–332.

Morlok A., Schiller B., Weber I., Daswani M. M., Stojic A. N., Reitze M. P., Gramse T., Wolters S. D., Hiesinger H., Grady M. M., and Helbert J. (2020). Mid-infrared reflectance spectroscopy

of carbonaceous chondrites and Calcium–Aluminum-rich inclusions. *Planetary and Space Science* **193**, 105078.
Moriarty G. M., Rumble D. III, and Friedrich J. M. (2009) Compositions of four unusual CM or CM-related Antarctic chondrites. *Geochemistry* **69**, 161–168.
Mouti Al-Hashimi X., Davidson J., Schrader D. L., and Bullock E. S. (2023) Fine-grained chondrule rims in Mighei-like carbonaceous chondrites: Evidence for a nebular origin and modification by impacts and recurrent solar radiation heating. *Meteorit. Planet. Sci.,* DOI: 10.1111/maps.14076
Nakamura T., Noguchi T., Zolensky M. E., and Tanaka M. (2003) Mineralogy and noble-gas signatures of the carbonate-rich lithology of the Tagish Lake carbonaceous chondrite: evidence for an accretionary breccia. *Earth Planet. Sci. Lett.* **207**, 83–101.
Nakamura T., Ikeda H., Kouyama T. Nakagawa H., Kusano H., Senshu H., Kameda S., Matsumoto K., Gonzalez-Franquesa F., Ozaki N., Takeo Y., Baresi N., Oki Y., Lawrence D. J., Chabot N. L., Peplowski P. N., Antonietta Barucci M., Sawyer E., Yokota S., Terada N., Ulamec S., Michel P., Kobayashi M., Sasaki S., Hirata N., Wada K., Miyamoto H., Imamura T., Ogawa N., Ogawa K., Iwata T., Imada T., Otake H., Canalias E., Lorda L., Tardivel S., Mary S., Kunugi M., Mitsuhashi S., Doressoundiram A., Merlin F., Fornasier S., Reess J-M., Bernardi P., Imai S., Ito Y., Ishida H., Kuramoto K. and Kawakatsu Y. (2021) Science operation plan of Phobos and Deimos from the MMX spacecraft. *Earth, Planets and Space* **73**, 227.
Naldrett A. J. (1989) Magmatic Sulphide Deposits. Oxford University Press, Oxford.
Petitat M., Birck J.-L., Luu T. H., and Gounelle M. (2011) The chromium isotopic composition of the ungrouped carbonaceous chondrite Tagish Lake. *Astrophys. J.* **736**, 23.
Pinto G. A., Jacquet E., Corgne A., Olivares F., Villeneuve J., and Marrocchi Y. (2024) Deciphering recycling processes during solar system evolution from magnesium-rich relict olivine grains in type II chondrules. *Geochim. Cosmochim. Acta* **364**, 65–78.
Poggiali G., Brucato J. R., Dotto E., Ieva S., Barucci M. A., and Pajola M. (2021) Temperature dependent mid-infrared (5–25 μm) reflectance spectroscopy of carbonaceous meteorites and minerals: Implication for remote sensing in Solar System exploration. *Icarus* **354**, 114040.
Qin L., Alexander C. M. O. D., Carlson R. W., Horan M. F. and Yokoyama T. (2010) Contributors to chromium isotope variation of meteorites. *Geochim. Cosmochim. Acta* **74**, 1122–1145.
Raghavan V. (2004) Fe–Ni–S (iron–nickel–sulfur). *J. Phase Equilib.* **25**, 373–381.
Rayner J. T., Toomey, D.W., Onaka, P.M., Denault, A.J., Stahlberger, W.E., Vacca, W.D., Cushing M.C., Wang, S. (2003) SPeX: A medium-resolution 0.8-5.5 microns spectrograph and imager for the NASA Infrared Telescope Facility. *Publications of the Astronomical Society of the Pacific*, 115, 362-382.
Render J., Bryson J. F. J., Ebert S., and Brennecka G. A. (2022) Disk transport rates from Ti isotopic signatures of refractory inclusions. *Meteorit. Planet. Sci.* **57**, 2158–2169.
Rubin A. E. (1989) Size-Frequency Distributions of Chondrules in CO3 Chondrites. *Meteoritics* **24**, 179–189.
Rüfenacht M., Morino P., Lai Y-J., Fehr M. A., Haba M. K., and Schönbächler M. (2023) Genetic relationships of solar system bodies based on their nucleosynthetic Ti isotope compositions and sub-structures of the solar protoplanetary disk. *Geochim. Cosmochim. Acta* **355**, 110–125.

Ruzicka A., Grossman J., Bouvier A., Herd C. D. K., and Agee C. B (2015) The Meteoritical Bulletin, No. 102. *Meteorit. Planet. Sci.* **50**, 1662.

Sanborn M. E., Wimpenny J., Williams C. D., Yamakawa A., Amelin Y., Irving A. J. and Yin Q. Z. (2019) Carbonaceous achondrites Northwest Africa 6704/6693: Milestones for early Solar System chronology and genealogy. *Geochim. Cosmochim. Acta* **245**, 577–596.

Schrader D. L. and Davidson J. (2017) CM and CO chondrites: A common parent body or asteroidal neighbors? Insights from chondrule silicates. *Geochim. Cosmochim. Acta* **214**, 157–171.

Schrader D. L. and Davidson J. (2022) Prolonged early migration of dust from the inner Solar System to the comet-forming region. *Earth Planet. Sci. Lett.* **589**, 117552.

Schrader D. L., Franchi I. A., Connolly, Jr., H. C., Greenwood R. C., Lauretta D. S. and Gibson J. M. (2011) The formation and alteration of the Renazzo-like carbonaceous chondrites I: Implications of bulk-oxygen isotopic composition. *Geochim. Cosmochim. Acta* **75**, 308–325.

Schrader D. L., Connolly, Jr., H. C., Lauretta D. S., Nagashima K., Huss G. R., Davidson J. and Domanik K. J. (2013) The formation and alteration of the Renazzo-like carbonaceous chondrites II: Linking O-isotope composition and oxidation state of chondrule olivine. *Geochim. Cosmochim. Acta* **101**, 302–327.

Schrader D. L., Davidson J., Greenwood R. C., Franchi I. A., and Gibson J. M. (2014) A water-ice rich minor body from the early Solar System: The CR chondrite parent asteroid. *Earth Planet. Sci. Lett.* **407**, 48–60.

Schrader D. L., Connolly H. C. Jr., Lauretta D. S., Zega T. J., Davidson J. and Domanik K. J. (2015) The formation and alteration of the Renazzo-like carbonaceous chondrites III: Towards understanding the genesis of ferromagnesian chondrules. *Meteorit. Planet. Sci.* **50**, 15–50.

Schrader D. L., Davidson J., and McCoy T. J. (2016) Widespread evidence for high-temperature formation of pentlandite in chondrites. *Geochim. Cosmochim. Acta* **189**, 359–376.

Schrader D. L., Nagashima K., Krot A. N., Ogliore R. C., Yin Q.-Z., Amelin Y. A., Stirling C. H. and Kaltenbach A. (2017) Distribution of ^{26}Al in the CR chondrite chondrule-forming region of the protoplanetary disk. *Geochim. Cosmochim. Acta.* **201**, 275–302.

Schrader D. L., Nagashima K., Waitukaitis S. R., Davidson J., McCoy T. J., Connolly, Jr., H. C. and Lauretta D. S. (2018a) The retention of dust in protoplanetary disks: Evidence from agglomeratic olivine chondrules from the outer Solar System. *Geochim. Cosmochim. Acta.* **223**, 405–421.

Schrader D. L., Fu R. R., Desch S. J. and Davidson J. (2018b) The background temperature of the protoplanetary disk within the first four million years of the Solar System. *Earth Planet. Sci. Lett.* **504**, 30–37.

Schrader D. L., Nagashima K., Davidson J., McCoy T. J., Ogliore R. C., and Fu R. R. (2020) Outward migration of chondrule fragments in the Early Solar System: O-isotopic evidence for rocky material crossing the Jupiter Gap? *Geochim. Cosmochim. Acta* **282**, 133–155.

Schrader D. L., Davidson J., McCoy T. J., Zega T. J., Russell S. S., Domanik K. J., and King A. J. (2021) The Fe/S ratio of pyrrhotite group sulfides in chondrites: An indicator of oxidation and implications for return samples from asteroids Ryugu and Bennu. *Geochim. Cosmochim. Acta* **303**, 66–91.

Sessions A. L., Burgoyne T. W., and Hayes J. M. (2001) Determination of the H-3 factor in hydrogen isotope ratio monitoring mass spectrometry. *Analytical Chemistry* **73**, 200–207.

Shields W. R., Murphy J. T., Cantazaro E. J. and Garner E. L. (1966) Absolute isotopic abundance ratios and the atomic weight of a reference sample of chromium. *J. Res. Natl. Bur. Stand.* **70A**, 193–197.

Shukolyukov A. and Lugmair G. W. (2006) Manganese-chromium isotope systematics of carbonaceous chondrites. *Earth Planet. Sci. Lett.* **250**, 200–213.

Tenner T. J., Nakashima D., Ushikubo T., Kita N. T. and Weisberg M. K. (2015) Oxygen isotope ratios of FeO-poor chondrules in CR3 chondrites: Influence of dust enrichment and H_2O during chondrule formation. Geochim. Cosmochim. Acta 148, 228–250.

Tenner T. J., Ushikubo T., Nakashima D., Schrader D. L., Weisberg M. K., Kimura M., and Kita N. T. (2018) Oxygen isotope characteristics of chondrules from recent studies by secondary ion mass spectrometry. In: Russell, S., Connolly Jr. H.C., Krot, A.N. (Eds.), Chondrules. Cambridge University Press, pp. 196–246.

Tholen D. J. (1989) Asteroid taxonomic classifications. In Asteroids II (ed. By R.P. Binzel et al.). Tucson, Univ. Arizona Press, pp. 1139–1150.

Thompson, M. S., Morris, R. V., Clemett, S. J., Loeffler, M. J., Trang, D., Keller, L. P., Christoffersen, R., Agresti, D. G. (2020). The effect of progressive space weathering on the organic and inorganic components of a carbonaceous chondrite. *Icarus* **346**, 113775.

Tonui E., Zolensky M., Hiroi T., Nakamura T., Lipschutz M. E., Wang M-S., and Okudaira K. (2014) Petrographic, chemical and spectroscopic evidence for thermal metamorphism in carbonaceous chondrites I: CI and CM chondrites. *Geochim. Cosmochim. Acta* **126**, 284–306.

Torrano Z. A., Brennecka G. A., Williams C. D., Romaniello S. J., Rai V. K., Hines R. R. and Wadhwa M. (2019) Titanium isotope signatures of calcium-aluminum-rich inclusions from CV and CK chondrites: Implications for early Solar System reservoirs and mixing. *Geochim. Cosmochim. Acta* **263**, 13–30.

Torrano Z. A., Schrader D. L., Davidson J., Greenwood R. C., Dunlap D. R., and Wadhwa M. (2021) The relationship between CM and CO chondrites: Insights from combined analyses of titanium, chromium, and oxygen isotopes in CM, CO, and ungrouped chondrites. *Geochim. Cosmochim. Acta* **301**, 70–90.

Trinquier A., Birck J.-L. and Allègre C. J. (2007) Widespread ^{54}Cr heterogeneity in the inner solar system. *Astrophys. J.* **655**, 1179–1185.

Trinquier A., Elliott T., Ulfbeck D., Coath C., Krot A. N. and Bizzarro M. (2009) Origin of nucleosynthetic isotope heterogeneity in the solar protoplanetary disk. *Science* **324**, 374–376.

Vacher L.G., Piani L., Rigaudier T., Thomassin D., Florin G., Piralla M., Marrocchi Y. (2020) Hydrogen in chondrites: influence of parent body alteration and atmospheric contamination on primordial components. *Geochim. Cosmochim. Acta* **281**, 53–66.

van Kooten E., Cavalcante L., Wielandt D., and Bizzarro M. (2020) The role of Bells in the continuous accretion between the CM and CR chondrite reservoirs. *Meteorit. Planet. Sci.* **55**, 575–590.

Vernazza P., Fulvio D., Brunetto R., Emery J. P., Dukes C. A., Cipriani F., Witasse O., Schaible M. J., Zanda B., Strazzulla G. and Baragiola R. A. (2013). Paucity of Tagish Lake-like parent bodies in the Asteroid Belt and among Jupiter Trojans. *Icarus* **225(1)**, 517–525.

Vilas F. and Smith B. A. (1985) Reflectance spectrophotometry (~0.5–1.0 μm) of outer-belt asteroids: Implications for primitive, organic solar system material. *Icarus* 64**,** 503–516.

Ushikubo T. and Kimura M. (2021) Oxygen-isotope systematics of chondrules and olivine fragments from Tagish Lake C2 chondrite: Implications of chondrule-forming regions in protoplanetary disk. *Geochim. Cosmochim. Acta* **293**, 328–343.

Wanas H. A. and Sallam E. (2016) Abiotically-formed, primary dolomite in the mid-Eocene lacustrine succession at Gebel El-Goza El-Hamra, NE Egypt: An approach to the role of smectitic clays. *Sedimentary Geology 343*, 132–140.

Weisberg M. K. and Huber H. (2007) The GRO 95577 CR1 chondrite and hydration of the CR parent body. *Meteorit. Planet. Sci.* **42**, 1495–1503.

Weisberg M. K., Prinz M., Clayton R. N. and Mayeda T. K. (1993) The CR (Renazzo-type) carbonaceous chondrite group and its implications. *Geochim. Cosmochim. Acta* **57**, 1567–1586.

Weisberg M. K., McCoy T. J. and Krot A. N. (2006) Systematic and evaluation of meteorite classification. In Meteorites and the Early Solar System II (eds. Lauretta D. S. and McSween H. Y.), pp. 19–52.

Williams C. D., Sanborn M. E., Defouilloy C., Yin Q.-Z., Kita N. T., Ebel D. S., Yamakawa A. and Yamashita K. (2020) Chondrules reveal large-scale outward transport of inner Solar System materials in the protoplanetary disk. *Proc. Natl. Acad. Sci.* **117**, 23426–23435.

Yabuta H., Alexander C. M. O'D., Fogel M. L., Kilcoyne A. L. D., and Cody G. D. (2010) A molecular and isotopic study of the macromolecular organic matter of the ungrouped C2 WIS 91600 and its relationship to Tagish Lake and PCA 91008. *Meteorit. Planet. Sci.* **45**, 1446–1460.

Yamada M., Sasaki S., Nagahara H., Fujiwara A., Hasegawa S., Yano H., Hiroi T., Ohashi H., and Otake H. (1999) Simulation of space weathering of planet-forming materials: Nanosecond pulse laser irradiation and proton implantation on olivine and pyroxene samples. *Earth, Planets and Space* **51**, 1255–1265.

Yamanobe M., Nakamura T., and Nakashima D. (2018) Oxygen isotope reservoirs in the outer asteroid belt inferred from oxygen isotope systematics of chondrule olivines and isolated forsterite and olivine grains in Tagish Lake-type carbonaceous chondrites, WIS 91600 and MET 00432. *Polar Sci.* **15**, 29–38.

Yamashita K., Maruyama S., Yamakawa A. and Nakamura E. (2010) ^{53}Mn–^{53}Cr chronometry of CB chondrite: Evidence for uniform distribution of ^{53}Mn in the early Solar System. *Astrophys. J.* **723**, 20–24.

Yesiltas M., Kebukawa Y., Glotch T. D., Zolensky M., Fries M., Aysal N., and Tukel F. S. (2022) Compositional and spectroscopic investigation of three ungrouped carbonaceous chondrites. *Meteorit. Planet. Sci.* **57**, 1665–1687.

Yokoyama T., Nagashima K., Kakai I., Young E. D., Abe Y., Aléon J., Alexander C. M.O'D., Amari S., Amelin Y., Bajo K-I., Bizzarro M., Bouvier A., Carlson R. W., Chaussidon M., Choi B-G., Dauphas N., Davis A. M., Di Rocco T., Fujiya W., Fukai R., Gautam I., Haba M. K., Hibiya Y., Hidaka H., Homma H., Hoppe P., Huss G. R., Ichida K-R., Iizuka T., Ireland T. R., Ishikawa A., Ito M., Itoh S., Kawasaki N., Kita N. T., Kitajima K., Kleine T., Komatani S., Krot A. N., Liu M-C., Masuda Y., McKeegan K. D., Morita M., Motomura K., Moynier F., Nguyen A., Nittler L., Onose M., Pack A., Park C., Piani L., Qin L., Russell S. S., Sakamoto N., Schönbächler M., Tafla L., Tang H., Terada K., Terada Y., Usui T., Wada S., Wadhwa M., Walker R. J., Yamashita K., Yin Q-Z., Yoneda S., Yui H., Zhang A-C., Connolly H. C. Jr., Lauretta D. S., Nakamura T., Naraoka H., Noguchi T., Okazaki R., Sakamoto K., Yabuta H., Abe M., Arakawa M., Fujii A., Hayakawa, Hirata N., Hirata N., Honda R., Honda C., Hosoda S., Iijima Y-I., Ikeda H., Ishiguro M., Ishihara Y., Iwata T., Kawahara K., Kikuchi S., Kitazato K., Matsumoto K., Matsuoka M., Michikami T., Mimasu Y., Miura A., Morota T., Nakazawa S., Namiki N., Noda H., Noguchi R., Ogawa N., Ogawa K., Okada T., Okamoto C., Ono G.,

Ozaki M., Saiki T., Sakatani N., Sawada H., Sunshu H., Shimaki Y., Shirai K., Sugita S., Takei Y., Takeuchi H., Tanaka S., Tatsumi E., Terui F., Tsuda Y., Tsukizaki R., Wada K., Watanabe S-I., Yamada M., Yamada T., Yamamoto Y., Kumagai K., Miyazaki A., Nakato A., Nishimura M., Soejima H., Suzuki A., Yada T., Yamamoto D., Yogata K., Yoshitake M., Tachibana S., and Yurimoto H. (2022) Samples returned from the asteroid Ryugu are similar to Ivuna-type carbonaceous meteorites. *Science* **379**, 6634. 10.1126/science.abn7850.

Yokoyama T., Wadhwa M., Iizuka T., Rai V., Gautam I., Hibiya Y., Masuda Y., Haba M. K.,Fukai R., Hines R., Phelan N., Abe Y., Aléon J., Alexander C. M. O'D., Amari S., Amelin Y., Bajo K., Bizzarro M., Bouvier A., Carlson R. W., Chaussidon M., Choi B-G. Dauphas N., Davis A. M., Di Rocco T., Fujiya W., Hidaka H., Homma H., Hoppe P., Huss G. R., Ichida K., Ireland T., Ishikawa A., Itoh S., Kawasaki N., Kita N. T., Kitajima K., Kleine T., Komatani S., Krot A. N., Liu M-C., McKeegan K. D., Morita M., Motomura K., Moynier F., Nakai I., Nagashima K., Nguyen A., Nittler L., Onose M., Pack A., Park C., Piani L, Qin L., Russell S., Sakamot N., Schönbächler M., Tafla L., Tang H., Terada K., Terada Y., Usui T., Wada S., Walker R. J., Yamashita K., Yin Q-Z., Yoneda S., Young E. D., Yui H., Zhang A-C., Nakamura T., Naraoka H., Noguchi T., Okazaki R., Sakamoto K., Yabuta H., Abe M., Miyazaki A., Nakato A., Nishimura M., Okada T., Yada T., Yogata K., Nakazawa S., Saiki T., Tanaka S., Terui F., Tsuda Y., Watanabe S., Yoshikawa M., Tachibana S., and Yurimoto H. (2023) Water circulation in Ryugu asteroid affected the distribution of nucleosynthetic isotope anomalies in returned sample. *Sci. Adv.* **9**, eadi7048.

Zhang J. J., Dauphas N., Davis A. M., and Pourmand A. (2011) A new method for MC-ICPMS measurement of titanium isotopic composition: Identification of correlated isotope anomalies in meteorites. *J. Anal. Atom. Spectrom.* **26**, 2197-2205.

Zhang J., Dauphas N., Davis A. M., Leya I. and Fedkin A. (2012) The proto-Earth as a significant source of lunar material. *Nature Geosci.* **5**, 251–255.

Zhu K., Moynier F., Schiller M., Alexander C. M. O'D., Davidson J., Schrader D. L., van Kooten E., and Bizzarro M. (2021) Chromium isotopic insights into the origin of chondrite parent bodies and the early terrestrial volatile depletion. *Geochim. Cosmochim. Acta* **301**, 158–186.

Zhu K., Schiller M., Moynier F., Groen M., Alexander C. M. O'D., Davidson J., Schrader D. L., Bischoff A., and Bizzarro M. (2023) Chondrite diversity revealed by chromium, calcium and magnesium isotopes. *Geochim. Cosmochim. Acta* **342**, 156–168.

Zolensky M. E., Nakamura K., Gounelle M., Mikouchi T., Kasama T., Tachikawa O., and Tonui E. (2002) Mineralogy of Tagish Lake: An ungrouped type 2 carbonaceous chondrite. *Meteorit. Planet. Sci.* **37**, 737–761.

TABLES

Table 1.
Apparent (2D) chondrule sizes, and chondrule textural and chemical types for Tarda and Tagish Lake.

Meteorite	Tarda ASU2149_C1	Tarda ASU2149_C2	Tarda ASU2149_C1+C2 (combined)	Tagish Lake ASU1684_C1
Sample area (mm^2)	18.5	32.8	51.3	125.4
Avg. Diameter (mm)	0.30	0.21	0.26	0.29
2σ (mm)	0.66	0.19	0.52	0.40
2SE (mm)	0.10	0.06	0.11	0.05
min. (mm)	0.11	0.07	0.07	0.05
max (mm)	1.30	0.41	1.30	1.37
Total # Chondrules	12	9	21	57
# (%) Porphyritic	12 (100%)	9 (100%)	21 (100%)	54 (94.7%)
# (%) Barred Olivine	0 (0%)	0 (0%)	0 (0%)	2 (3.5%)
# (%) Cryptocrystalline	0 (0%)	0 (0%)	0 (0%)	1 (1.8%)
# (%) FeO-poor	11 (91.7%)	7 (77.8%)	18 (85.7%)	52 (91.2%)
# (%) FeO-rich	1 (8.3%)	2 (22.2%)	3 (14.3%)	5 (8.8%)

Fragments of chondrules and single mineral grains were not included in chondrule size measurements.
% values are by number.

Table 2.
Modal abundances of chondrules and matrix, and modal mineralogy of Tarda and Tagish Lake.

Meteorite	Tarda ASU2149_C1	Tarda ASU2149_C2	Tarda ASU2149_C1+C2 (normalized)	Tagish Lake ASU1684_C1
Sample area (mm2)	18.5	32.8	51.3	125.4
Chondrules, CAIs, Matrix				
Chondrules (vol.%)	10.6	3.3	6.5	5.9
CAIs (vol.%)	0.0	0.4	0.2	0.3
Matrix (vol.%)	89.4	96.3	93.3	93.8
Total (vol.%)	100.0	100.0	100.0	100.0
Individual Minerals				
Olivine (vol.% ± σ)	4.41±0.49	2.44±0.37	3.30±0.30	4.11±0.31
Al-spinel (vol.% ± σ)	none	trace	trace	0.02±0.01
Ca-carbonate (vol.% ± σ)	3.76±0.56	2.85±0.34	3.24±0.33	3.20±0.83
Phosphate (vol.% ± σ)	0.23±0.09	0.10±0.04	0.15±0.05	trace
Chromite (vol.% ± σ)	trace	trace	trace	trace
Fe,Ni Metal (vol.% ± σ)	trace	trace	trace	trace
Magnetite (vol.% ± σ)	4.30±0.39	3.88±0.43	4.06±0.36	4.59±0.63
Fe-sulfide (vol.% ± σ)	1.45±0.34	3.04±0.82	2.35±0.40	1.86±0.81
Total Identified Minerals (vol.% ± σ)	14.15±1.07	12.33±1.11	13.12±0.78	13.79±1.59
Mean Deficit from 100 vol.% ≈ Phyllosilicate Abundance (vol.%)	85.85	87.67	86.88	86.21

No pyroxene, plagioclase/glass, anorthite, or gypsum were identified in Tarda or Tagish Lake.
trace = abundance <0.01 vol.%
Mean Deficit from 100 vol.% = the estimated phyllosilicate abundance (e.g., Donaldson Hanna et al., 2019).
Tarda ASU2149_C1 and ASU2149_C2 combined abundances are area normalized to account for sample size differences.

Table 3.
Selected individual chondrule olivine analyses from Tarda and Tagish Lake.

Meteorite	Tarda ASU2149_C1	Tarda ASU2149_C1	Tarda ASU2149_C1	Tarda ASU2149_C2	Tarda ASU2149_C2	Tarda ASU2149_C2	Tagish Lake ASU1684_C1	Tagish Lake ASU1684_C1
Chondrule	Ch1	Ch5	Ch3	Ch1	Ch2	Ch9	Ch1	Ch7
Grain	G1	G2	G2	G1	G4	G1	G6	G5
Analysis #	26	92	72	3	25	49	36	119
Ch Type	dusty olivine	type I	type II	type II	type I	type II	type II	type I
Chemical Composition (wt.% oxides)								
P_2O_5	bdl	bdl	0.09	bdl	bdl	bdl	bdl	bdl
SiO_2	40.72	41.25	34.06	35.40	41.94	38.73	35.56	41.28
Al_2O_3	0.05	0.02	bdl	bdl	bdl	bdl	bdl	bdl
Cr_2O_3	0.35	0.49	0.30	0.18	0.37	0.38	0.26	0.43
FeO	3.18	1.61	44.40	35.39	0.74	15.15	34.89	0.76
MnO	0.13	0.16	0.55	0.36	0.12	0.20	0.29	0.15
MgO	53.99	57.16	19.85	27.54	57.26	44.42	28.66	56.67
CaO	0.19	0.15	0.67	0.42	0.26	0.30	0.21	0.21
NiO	bdl	bdl	0.14	0.19	bdl	0.16	0.16	bdl
Total	98.61	100.84	100.06	99.46	100.69	99.35	100.04	99.49
Cation formula based on four oxygens								
P	bdl	bdl	0.002	bdl	bdl	bdl	bdl	bdl
Si	0.983	0.970	0.996	0.992	0.983	0.984	0.988	0.979
Al	0.001	0.001	bdl	bdl	bdl	bdl	bdl	bdl
Cr	0.007	0.009	0.007	0.004	0.007	0.008	0.006	0.008
Fe	0.064	0.032	1.086	0.830	0.015	0.322	0.810	0.015
Mn	0.003	0.003	0.014	0.008	0.002	0.004	0.007	0.003
Mg	1.943	2.004	0.866	1.151	2.000	1.682	1.187	2.004
Ca	0.005	0.004	0.021	0.013	0.006	0.008	0.006	0.005

Ni	bdl	bdl	0.003	0.004	bdl	0.003	0.004	bdl
Total	3.006	3.023	2.996	3.002	3.013	3.011	3.007	3.014
Fa	3.2	1.6	55.6	41.9	0.7	16.1	40.6	0.7
Fo	96.8	98.4	44.4	58.1	99.3	83.9	59.4	99.3
Fe (afu)	0.064	0.032	1.086	0.830	0.015	0.322	0.810	0.015
Mn (afu)	0.003	0.003	0.014	0.008	0.002	0.004	0.007	0.003
Fe/Mg	0.03	0.02	1.25	0.72	0.01	0.19	0.68	0.01
Fe/Mn	25.0	9.7	80.4	98.3	5.9	75.1	118.8	5.0

Ch = chondrule; G = grain. bdl = below detection limit.

Standards and detection limits (in wt.%): albite for Na (0.03), apatite for P (0.02), diopside for Si (0.02), Mg (0.04), and Ca (0.01), anorthite for Al (0.02), orthoclase for K (0.02), rhodonite for Mn (0.05), rutile for Ti (0.02), fayalite for Fe (0.07), chromite for Cr (0.02), and nickel metal for Ni (0.07).

K, Ti, and Na were bdl in all analyses shown here. All analyses are provided in EA-1.

1418

Table 4.
Selected individual sulfide and metal analyses from Tarda and Tagish Lake.

Meteorite	Tarda ASU2149_C2	Tarda ASU2149_C1	Tarda ASU2149_C1	Tarda ASU2149_C2	Tarda ASU2149_C1	Tarda ASU2149_C2	Tagish Lake ASU1684_C1	Tagish Lake ASU1684_C1
Area	Ch2	OA5	-	-	OA5	-	MOA9	Ch4
Grain	G3	OA5	OA3	OA3	OA5	OA3		OA3
Analysis #	23	8	16	44	4	46	10	71
Mineral	Ni-poor metal	Pyrrhotite	Pyrrhotite	Pyrrhotite	Pentlandite	Pentlandite	Pyrrhotite	Pentlandite
Chemical Composition (wt.%)								
Fe	90.3	59.5	60.2	59.9	34.5	30.7	59.0	32.5
S	bdl	39.38	39.34	38.92	34.21	33.04	39.24	33.19
Si	0.21	bdl	bdl	bdl	bdl	0.03	0.14	0.29
P	1.17	bdl	bdl	bdl	bdl	bdl	bdl	bdl
Mn	bdl	bdl	0.04	bdl	bdl	bdl	0.04	bdl
Ni	6.2	1.0	0.1	1.1	30.5	35.0	1.7	32.1
Co	0.20	0.13	bdl	bdl	0.72	0.96	bdl	1.23
Cr	0.46	0.03	0.18	0.04	0.03	0.04	0.09	0.03
Mg	0.33	bdl	bdl	bdl	bdl	bdl	0.11	0.16
Al	0.03	bdl	bdl	bdl	bdl	bdl	bdl	bdl
Total	98.9	100.0	99.9	100.0	100.0	99.8	100.3	99.5
Chemical Composition (at.%)								
Fe	90.1	46.1	46.7	46.5	27.9	25.1	45.5	26.4
S	0.00	53.11	53.08	52.64	48.11	46.93	52.71	47.01
Si	0.42	bdl	bdl	bdl	bdl	0.05	0.22	0.46
P	2.11	bdl	bdl	bdl	bdl	bdl	bdl	bdl
Mn	bdl	bdl	0.03	bdl	bdl	bdl	0.03	bdl
Ni	5.9	0.7	0.1	0.8	23.4	27.2	1.2	24.8

Co	0.19	0.10	0.00	0.00	0.55	0.74	bdl	0.95
Cr	0.50	0.02	0.15	0.03	0.03	0.03	0.07	0.03
Mg	0.76	bdl	bdl	bdl	bdl	bdl	0.20	0.30
Al	0.07	bdl	bdl	bdl	bdl	bdl	bdl	bdl
Total	100.0	100.0	100.0	100.0	100.0	100.0	100.0	100.0
at.% ratios								
Fe/S (at.%)		0.87	0.88					
Cations/S (at.%)		0.88	0.88	0.90	1.08	1.13	0.89	1.11

Ch = chondrule; OA = opaque assemblage; MOA = matrix opaque assemblage. G = grain. bdl = below detection limit.
Fe/S for pyrrhotite if Ni< 1 wt.%.
Cations =Fe+Ni+Cr+Ti+Co+Cu.
Standards and detection limits (in wt.%): San Carlos olivine for Si (0.02) and Mg (0.02), indium phosphide for P (0.03), troilite for S (0.03) and Fe (0.11), chromite for Cr (0.02), chalcopyrite for Cu (0.12), Co-metal for Co (0.08), Ni-metal for Ni (0.11), anorthite for Al (0.02), Mn-metal for Mn (0.03), and rutile for Ti (0.02).
Ti and Cu are all below detection limits in analyses shown here. All analyses are provided in EA-1.

1436

Table 5.
Selected individual carbonate analyses from Tarda, Tagish Lake, Orgueil, and Kolang.

Meteorite	Tarda ASU2149_C1	Tarda ASU2149_C2	Tagish Lake ASU1684_C1	Tagish Lake ASU1684_C1	Orgueil USNM6765-2	Kolang ASU2147_C1	Kolang ASU2147_C3c	Kolang ASU2147_C3c
Type	C2-ung	C2-ung	C2-ung	C2-ung	CI	CM1/2 (host)	CM1-clast	CM1-clast
Grain	CC2	CC2	CC1	CC3	CC1	CC3	CC4	CC1
Analysis #	115	72	173	175	15	32	34	35
Mineral	dolomite	dolomite	dolomite	calcite	dolomite	dolomite	dolomite	calcite
Chemical Composition (wt.% oxides)								
Na2O	0.07	0.07	0.16	0.07	0.19	bdl	bdl	bdl
SiO2	0.77	0.20	bdl	0.16	bdl	0.41	0.13	bdl
MgO	16.30	20.32	15.20	0.17	21.25	19.27	18.92	bdl
P2O5	0.12	bdl	0.38	0.12	0.20	bdl	bdl	0.13
K2O	bdl	bdl	bdl	bdl	bdl	bdl	bdl	0.04
CaO	29.29	28.01	29.05	54.76	28.13	29.55	29.31	55.13
MnO	3.85	0.72	4.22	bdl	0.37	1.61	0.22	0.44
FeO	3.89	4.26	5.15	0.97	1.98	2.56	4.46	0.60
SO3	0.09	0.15	bdl	1.15	bdl	bdl	bdl	bdl
Cr2O3	bdl	0.19	bdl	bdl	bdl	bdl	bdl	bdl
CO2	45.46	45.93	45.79	42.46	47.82	46.49	46.77	43.52
Total	99.85	99.85	99.95	99.86	99.94	99.89	99.81	99.87
Cation formula based on three oxygens								
Na	0.002	0.002	0.005	0.002	0.006	bdl	bdl	bdl
Si	0.012	0.003	bdl	0.003	bdl	0.006	0.002	bdl
Mg	0.387	0.476	0.362	0.004	0.487	0.449	0.441	bdl
P	0.002	bdl	0.005	0.002	0.003	bdl	bdl	0.002
K	bdl	bdl	bdl	bdl	bdl	bdl	bdl	0.001
Ca	0.499	0.471	0.497	0.983	0.464	0.495	0.491	0.989
Mn	0.052	0.010	0.057	bdl	0.005	0.021	0.003	0.006

Fe	0.052	0.056	0.069	0.014	0.025	0.034	0.058	0.008
S	0.001	0.002	bdl	0.014	bdl	bdl	bdl	bdl
Cr	bdl	0.002	bdl	bdl	bdl	bdl	bdl	bdl
C	0.987	0.984	0.999	0.971	1.004	0.993	0.999	0.994
Sum	1.994	2.006	1.994	1.993	1.993	1.999	1.995	2.000
Normalized mol.%								
Fe+Mn	10.5	6.5	12.8	1.4	3.1	5.5	6.2	1.5
Ca	50.5	46.5	50.5	98.2	47.2	49.6	49.4	98.5
Mg	39.1	47.0	36.7	0.4	49.7	45.0	44.4	0.0

CC = carbonate grain. bdl = below detection limit.

Standards and detection limits (in wt.%): San Carlos olivine for Si (0.02), albite for Na (0.04), Mg-carbonate for Mg (0.05), anorthite for Al (0.02), apatite for P (0.03), K-feldspar for K (0.02), diopside for Ca (0.04), Mn-carbonate for Mn (0.08), fayalite for Fe (0.10), barite for S (0.02), Ni-metal for Ni (0.11), rutile for Ti (0.03), and chromite for Cr (0.03).

Al, Ni, Ti all bdl in analyses shown here. Included to check for beam overlap into other phases. All analyses are provided in EA-1.

Table 6.
The bulk H, C and N elemental and isotopic compositions of Tarda, Tagish Lake, and MET 00432.

Meteorite	Classification	H (wt.%) ± σ	δD (‰) ± σ	C (wt.%) ± σ	$\delta^{13}C$ (‰) ± σ	N (wt.%) ± σ	$\delta^{15}N$ (‰) ± σ	Reference
Tarda ASU2149	C2-ung	0.916 ± 0.010	607.9 ± 18.1	4.167 ± 0.034	8.0 ± 0.4	0.297 ± 0.003	62.04 ± 0.15	This study
Literature data								
Tarda 1	C2-ung	0.948	678.4					Marrocchi et al. (2021)
Tarda 2	C2-ung	0.952	681.6					Marrocchi et al. (2021)
Tarda 3	C2-ung			4.00	11.3	0.28	54.7	Marrocchi et al. (2021)
Tarda 4	C2-ung			4.06	10.7	0.28	55.3	Marrocchi et al. (2021)
Tarda 5	C2-ung			4.11	10.7	0.30	55.9	Marrocchi et al. (2021)
Tagish Lake 11i	C2-ung	0.738 ± 0.009	542.0 ± 8.7	3.95	14.0	0.17	59.7	Alexander et al. (2012)
Tagish Lake 11h	C2-ung	0.872 ± 0.004	556.6 ± 6.2	4.13	9.4	0.19	62.6	Alexander et al. (2012)
Tagish Lake 5b	C2-ung	0.945 ± 0.003	507.6 ± 4.0	4.11	10.1	0.24	76.2 ± 0.1	Alexander et al. (2012)
MET 00432	CM2	1.065 ± 0.020	45.3 ± 0.2	2.724 ± 0.021	3.0 ± 0.5	0.118 ± 0.004	29.8 ± 1.0	Alexander et al. (2012)

The uncertainties from this study and Alexander et al. (2012) are 1σ and are based on replicate analyses.

Table 7.
Cr and Ti isotope compositions measured for samples in this study.

Cr isotope compositions				
Sample	$\varepsilon^{53}Cr$	$\varepsilon^{54}Cr$		N
DTS-1	0.08±0.15	0.20±0.27		4
Allende	0.14±0.17	0.91±0.31		4
Tarda ASU2149	0.02 ± 0.14	1.14 ± 0.17		4
Ti isotope compositions				
Sample	$\varepsilon^{46}Ti$	$\varepsilon^{48}Ti$	$\varepsilon^{50}Ti$	N
BCR-2	-0.02 ± 0.11	0.02 ± 0.04	-0.16 ± 0.12	6
Allende	0.68 ± 0.08	-0.05 ± 0.07	2.99 ± 0.07	4
Tarda ASU2149	0.55 ± 0.10	-0.06 ± 0.03	2.94 ± 0.13	5

DTS-1 = dunite from Twin Sisters area, Hamilton, Washington Reference Material
BCR-2 = Columbia River Basalt Reference Material
Allende = Allende Smithsonian Reference Material
value ± 2SE; N = number of replicates.

Table 8.
Bulk Cr, Ti, and O isotopic compositions of Tarda and Tagish Lake.

Sample	Tarda	Tagish Lake
ε^{53}Cr	0.02	0.53
2SE	0.14	0.04
ε^{54}Cr	1.14	1.19
2SE	0.17	0.11
Cr reference	this study	Petitat et al. (2011)
ε^{50}Ti	2.94	2.76
2SE	0.13	0.26
Ti reference	this study	Trinquier et al. (2009)
Δ^{17}O	-0.284	-0.870
2SE	±0.053	± 0.38
O Reference	Gattacceca et al. (2021)	Grossman (2000)

For this study, sample was Tarda ASU2149, homogenized powder made from 1.03 g of interior chips. The same powder that was also used for H, C, and N analyses (Table 6).

1518

Table 9.
Bulk elemental abundances of Tarda ASU2149.

Element	Abundance (ppm)
Mg	98975
Al	9230
K	329
Ca	8943
Sc	5.87
Ti	469
V	55
Cr	2465
Mn	1377
Fe	161388
Co	456
Ni	9846
Cu	111
Zn	184
Ga	6.31
Sr	5.94
Zr	3.97
Nb	0.358
Mo	1.158
Rh	0.119
Cd	0.369
Te	1.13
Cs	0.1153
Ba	2.18
La	0.250
Ce	0.620
Nd	0.483
Sm	0.159
Eu	0.060
Gd	0.214
Tb	0.037
Dy	0.225
Ho	0.053
Er	0.168
Tm	0.026
Yb	0.172
Lu	0.024

Typical error is <10%.

1519
1520

FIGURES

Figure 1. Individual stones and fragments of Tarda in the Carleton B. Moore Meteorite Collection in the Buseck Center for Meteorite Studies at Arizona State University (a total of ~24 grams of material is shown).

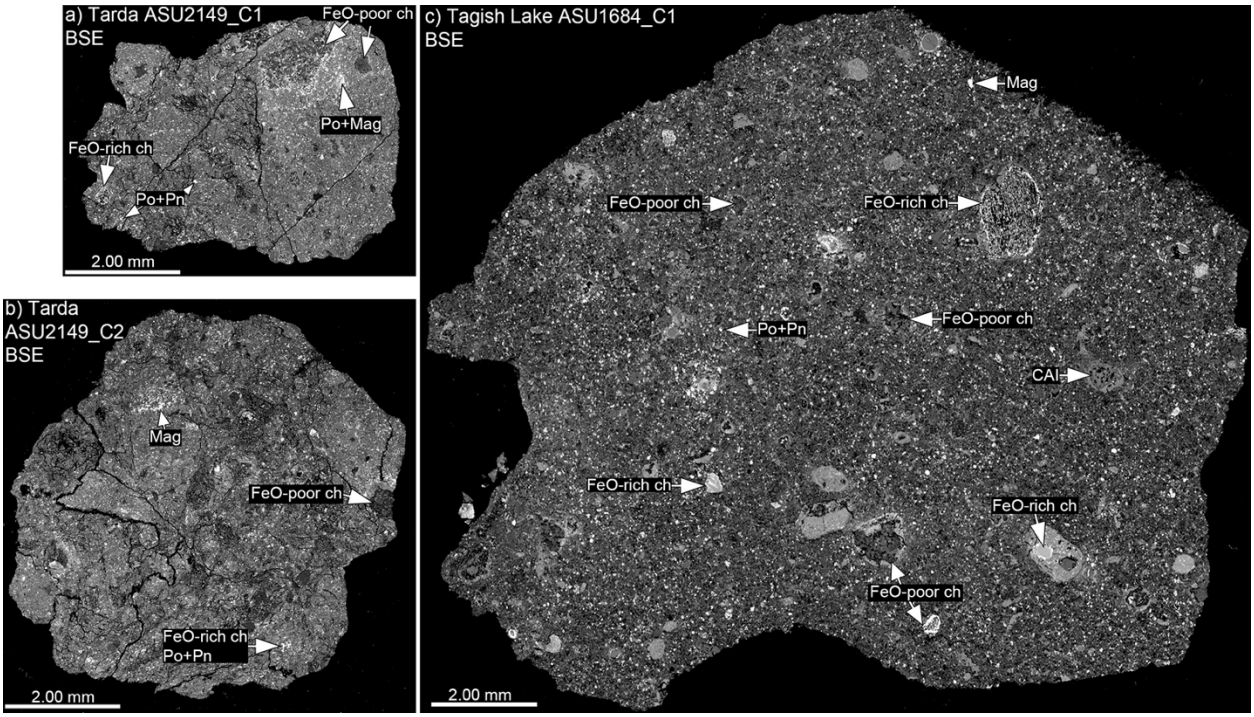

Figure 2. Full backscattered electron (BSE) images of (a) Tarda ASU2149_C1, (b) Tarda ASU2149_C2, and (c) Tagish Lake ASU1684_C1. All images are shown at the same scale for ease of comparison between samples. For sizes and modal mineralogy, see Tables 1 and 2. CAI = calcium aluminum rich inclusion, ch = chondrule, Po = pyrrhotite, Pn = pentlandite, and Mag = magnetite.

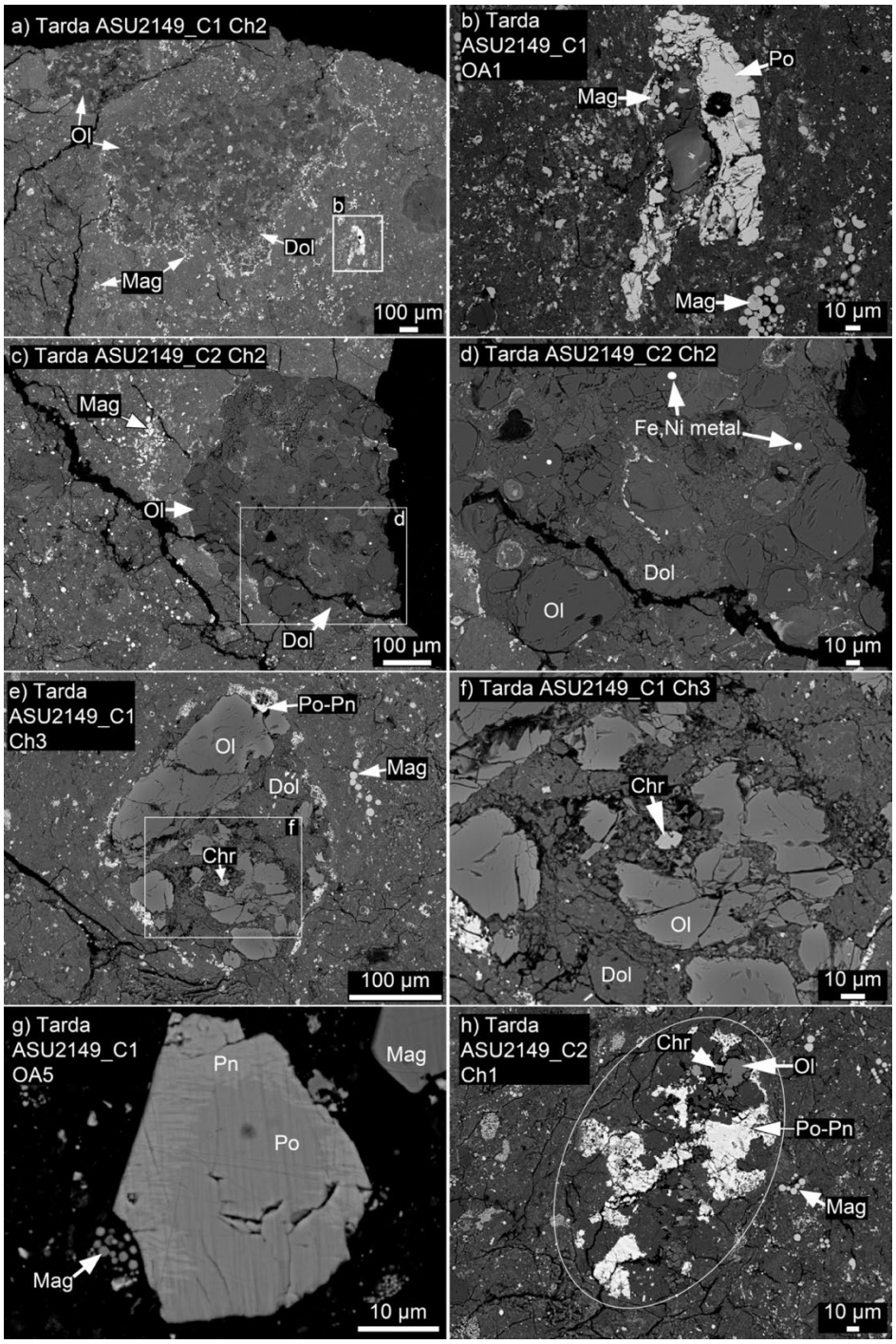

Figure 3. Back scattered electron (BSE) images of Tarda ASU2149_C1 and ASU2149_C2; (a,c) FeO-poor chondrules, an (e,f) FeO-rich chondrule, (a,b,c,e,g,h) magnetite (Mag), (b,g) including magnetite framboids, (b,e,g,h) pyrrhotite (Po) and pentlandite (Pn), (e) dolomite (Dol) and chromite (Chr) inside a partially replaced FeO-rich chondrule, and a (h) chondrule nearly completely replaced by phyllosilicates. Ch = chondrule. OA = opaque assemblage in the matrix. Ol = olivine.

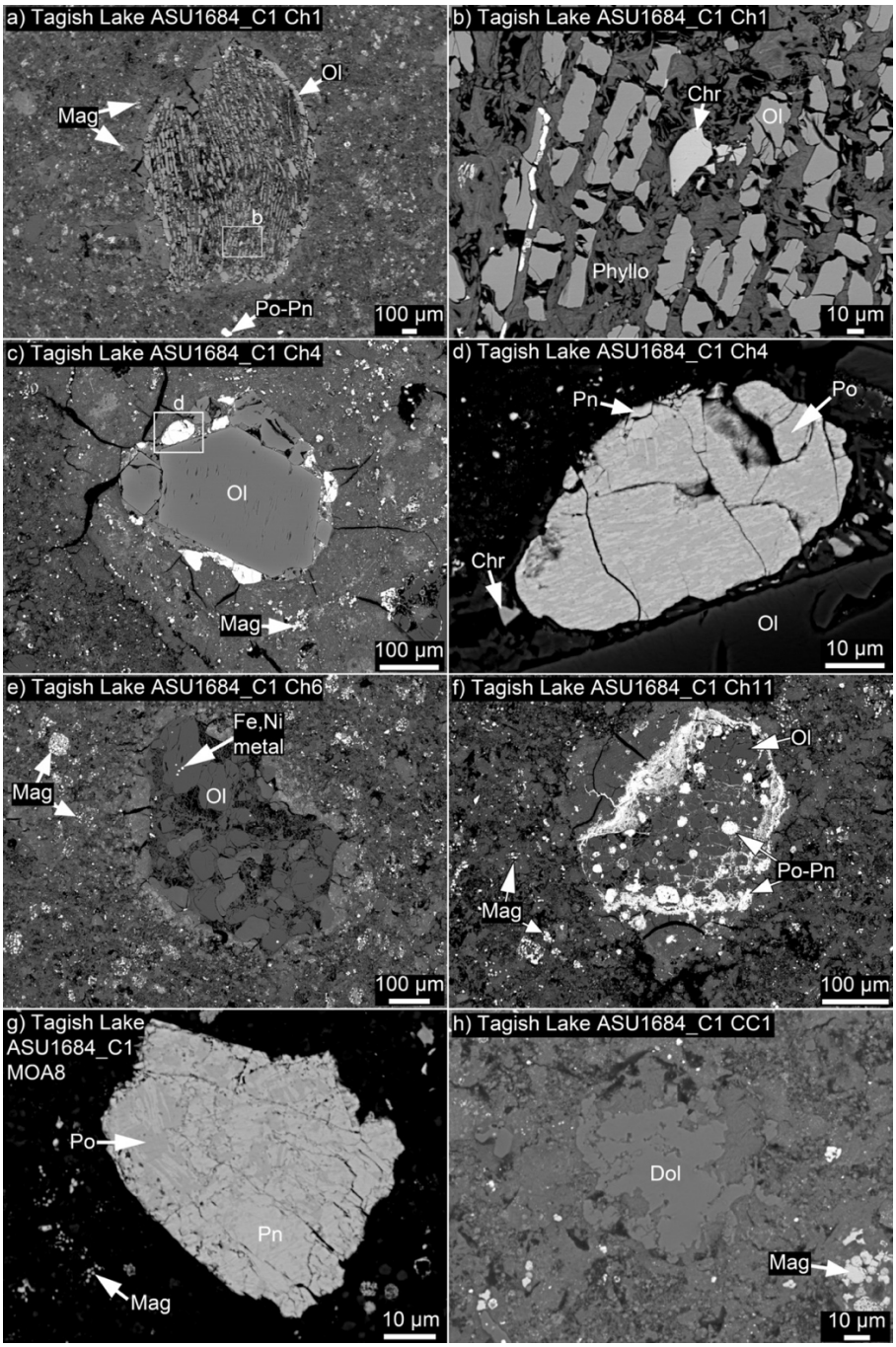

Figure 4. BSE images of Tagish Lake ASU1684_C1; (a,b) FeO-rich barred olivine chondrule containing olivine (Ol) and chromite (Chr), and phyllosilicates (Phyllo), (c) FeO-rich porphyritic olivine chondrule with pyrrhotite, pentlandite, and chromite, (e) FeO-poor porphyritic olivine chondrule containing Fe,Ni metal grains in olivine, (f) FeO-poor porphyritic olivine chondrule containing abundant pyrrhotite and pentlandite, (g) matrix opaque assemblage (MOA) consisting of pyrrhotite (Po) and pentlandite (Pn) with nearby magnetite (Mag) framboids, and a dolomite (Dol) in the matrix with nearby magnetite. Ch = chondrule.

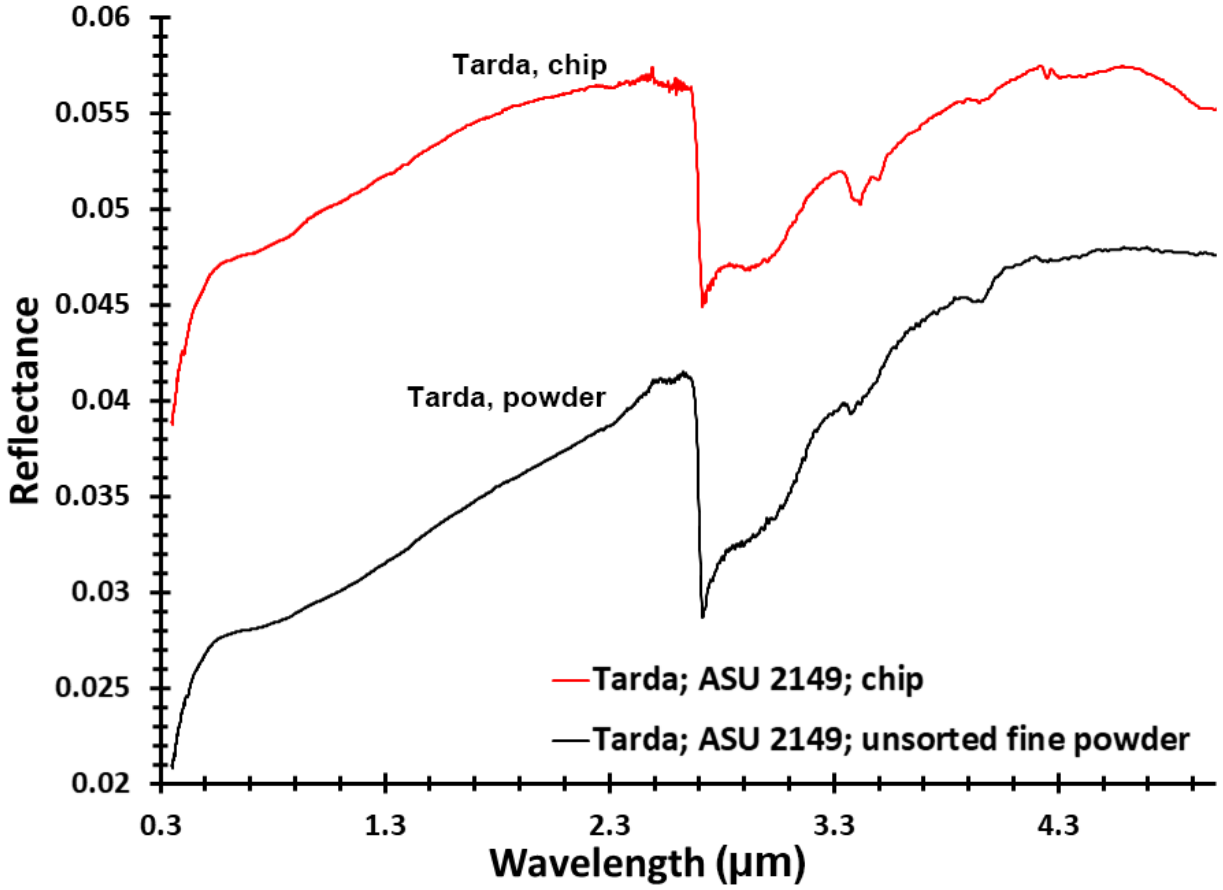

Figure 5. Reflectance spectra of a chip and unsorted fine powder of the Tarda meteorite. Spectra were measured at i=30° and e=0°. See text for details.

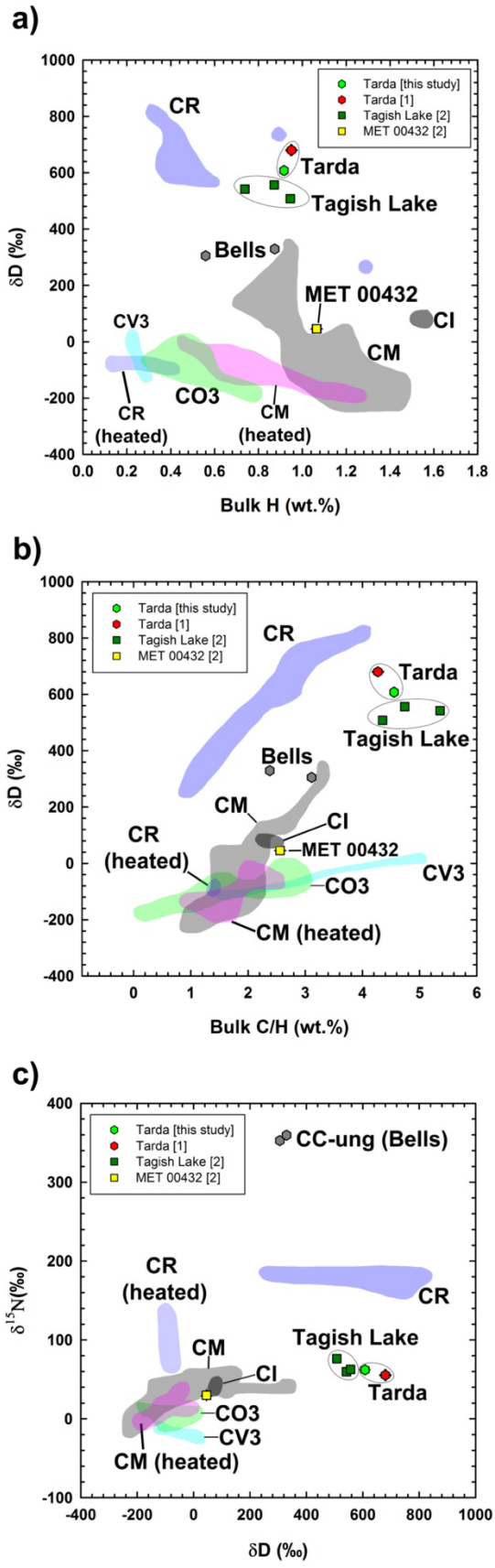
a)
Tarda [this study]
Tarda [1]
Tagish Lake [2]
MET 00432 [2]
CR
Tarda
Tagish Lake
Bells
MET 00432
CI
CV3
CM
CO3
CR (heated)
CM (heated)
δD (‰)
Bulk H (wt.%)
b)
Tarda [this study]
Tarda [1]
Tagish Lake [2]
MET 00432 [2]
CR
Tarda
Tagish Lake
Bells
CM
CI
CR (heated)
MET 00432
CV3
CO3
CM (heated)
δD (‰)
Bulk C/H (wt.%)
c)
Tarda [this study]
Tarda [1]
Tagish Lake [2]
MET 00432 [2]
CC-ung (Bells)
CR (heated)
CR
Tagish Lake
CM
CI
Tarda
CO3
CV3
CM (heated)
δ15N(‰)
δD (‰)

1601

Figure 6. The bulk H, C, and N isotopic compositions and abundances of Tarda (this study), compared to literature data from Tarda (average values from [1] Marrocchi et al., 2021), Tagish Lake and MET 00432 (from [2] Alexander et al., 2012), the ungrouped carbonaceous chondrite Bells from [2], and the CO, CM (heated and unheated), CV, CR (heated and unheated), and CI chondrites. (a) Bulk H (wt.%) vs. δD (‰); (b) Bulk C/H (wt.%) vs. δD (‰); (c) δD (‰) vs. $\delta^{15}N$ (‰). Tarda is most similar to Tagish Lake, and not like any other meteorite or meteorite group. For direct comparison, the chondrite fields shown are from data collected using the same technique as for Tarda in this study: CM chondrites (Alexander et al., 2012); heated CM chondrites (Alexander et al., 2012); CR chondrites (Alexander et al., 2012; Davidson et al., 2019b); heated CR chondrites (Alexander et al., 2013); CV3 chondrites (Alexander et al., 2012; Davidson et al., 2014); CO3 chondrites (Alexander et al., 2012; Alexander et al., 2018), and CI chondrites (Alexander et al., 2012).

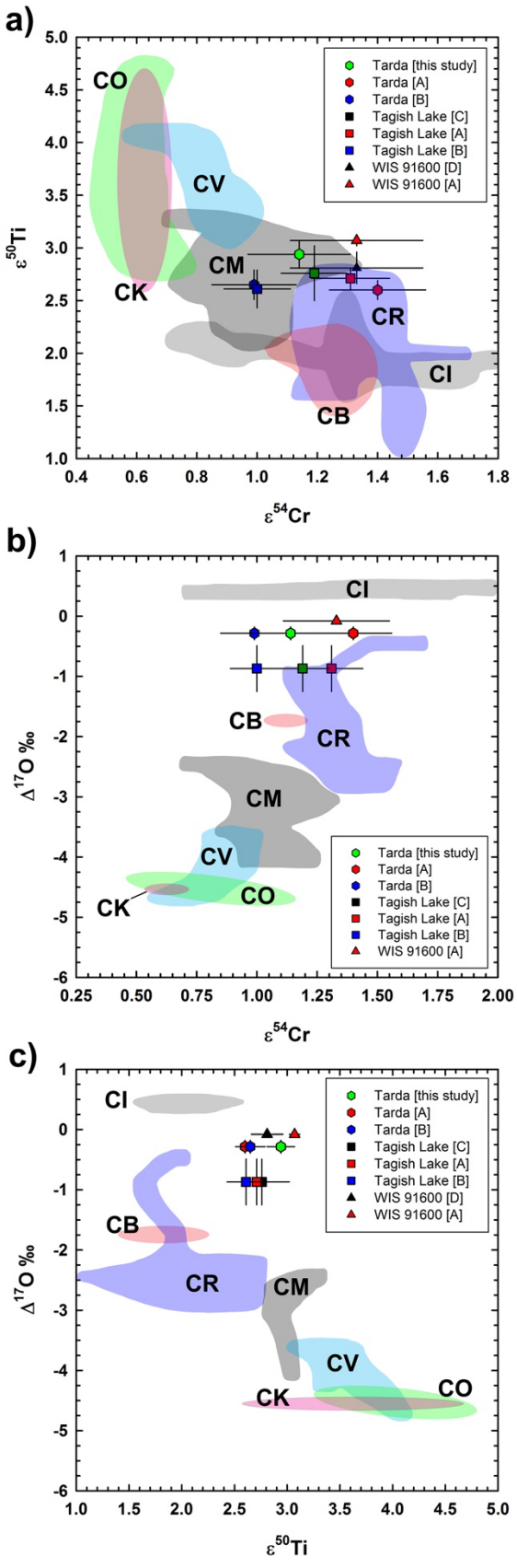
a)
CO
CV
CM
CK
CR
CI
CB
Tarda [this study]
Tarda [A]
Tarda [B]
Tagish Lake [C]
Tagish Lake [A]
Tagish Lake [B]
WIS 91600 [D]
WIS 91600 [A]
ε50Ti
ε54Cr
b)
CI
CB
CR
CM
CV
CO
CK
Δ17O ‰
ε54Cr
c)
CI
CB
CR
CM
CV
CK
CO
Δ17O ‰
ε50Ti

1617

Figure 7. $\varepsilon^{54}Cr$, $\varepsilon^{50}Ti$, and $\Delta^{17}O$ isotopic compositions of Tarda compared to literature values data for Tarda, Tagish Lake, WIS 91600, and fields for CO, CM, CV, CK, CR, and CI chondrites [1–25]. (a) $\varepsilon^{54}Cr$ vs. $\varepsilon^{50}Ti$ (b) $\varepsilon^{54}Cr$ vs. $\Delta^{17}O$ (c) $\varepsilon^{50}Ti$ vs. $\Delta^{17}O$. The $\varepsilon^{54}Cr$ and $\varepsilon^{50}Ti$ values for Tarda are this study, while $\Delta^{17}O$ for Tarda is from Gattacceca et al. (2021). Uncertainties on Tarda, Tagish Lake, and WIS 91600 are ±2SE (e.g., Table 7). [A] Literature data for Tarda, Tagish Lake, and WIS 91600 plotted for comparison ($\varepsilon^{54}Cr$ and $\varepsilon^{50}Ti$, Hellman et al., 2023; $\Delta^{17}O$ for Tarda, Gattacceca et al., 2021; $\Delta^{17}O$ for Tagiah Lake, Grossman, 2000; and $\Delta^{17}O$ for WIS 91600, Clayton and Mayeda, 2003). [B] Literature data for Tarda and Tagish Lake plotted for comparison ($\varepsilon^{54}Cr$ and $\varepsilon^{50}Ti$, Yokoyama et al., 2023; $\Delta^{17}O$ for Tarda, Gattacceca et al., 2021; and $\Delta^{17}O$ for Tagiah Lake, Grossman, 2000). [C] Literature data for Tagish Lake plotted for comparison ($\varepsilon^{54}Cr$, Petitat et al., 2011; $\varepsilon^{50}Ti$, Trinquier et al., 2009; and $\Delta^{17}O$, Grossman, 2000). [D] Literature data for WIS 91600 plotted for comparison ($\varepsilon^{54}Cr$, Hellman et al., 2023; $\varepsilon^{50}Ti$, Render et al., 2022; and $\Delta^{17}O$, Clayton and Mayeda, 2003). The $\varepsilon^{54}Cr$, $\varepsilon^{50}Ti$, and $\Delta^{17}O$ data used to construct the compositional fields for the CO [1–4,7,16], CM [2,3,4,6,10,16,18–21], CV [1–4,6,7,9,10,18,22], CK [2,3,4,7], CR [2,4,7,8,9,10,13,18,23], CB [2,3,5], and CI [1–4,9,10,18,23,24,25] chondrites are: [1] Shukolyukov and Lugmair (2006); [2] Trinquier et al. (2007); [3] Trinquier et al. (2009); [4] Qin et al. (2010); [5] Yamashita et al. (2010); [6] Zhang et al. (2011); [7] Zhang et al. (2012); [8] Sanborn et al. (2019); [9] Weisberg et al. (1993); [10] Clayton and Mayeda (1999); [11] Greenwood and Franchi (2004); [12] Greenwood et al. (2010); [13] Schrader et al. (2011); [14] Hewins et al. (2014); [15] Jacquet et al. (2016); [16] Williams et al. (2020); [17] Torrano et al. (2021); [18] Rüfenacht et al. (2023); [19] Göpel et al. (2015); [20] Ruzicka et al. (2015); [21] van Kooten et al. (2020); [22] Zhu et al. (2021); [23]; Hellman et al. (2023); [24] Kadlag et al. (2019); [25] Yokoyama et al. (2023).

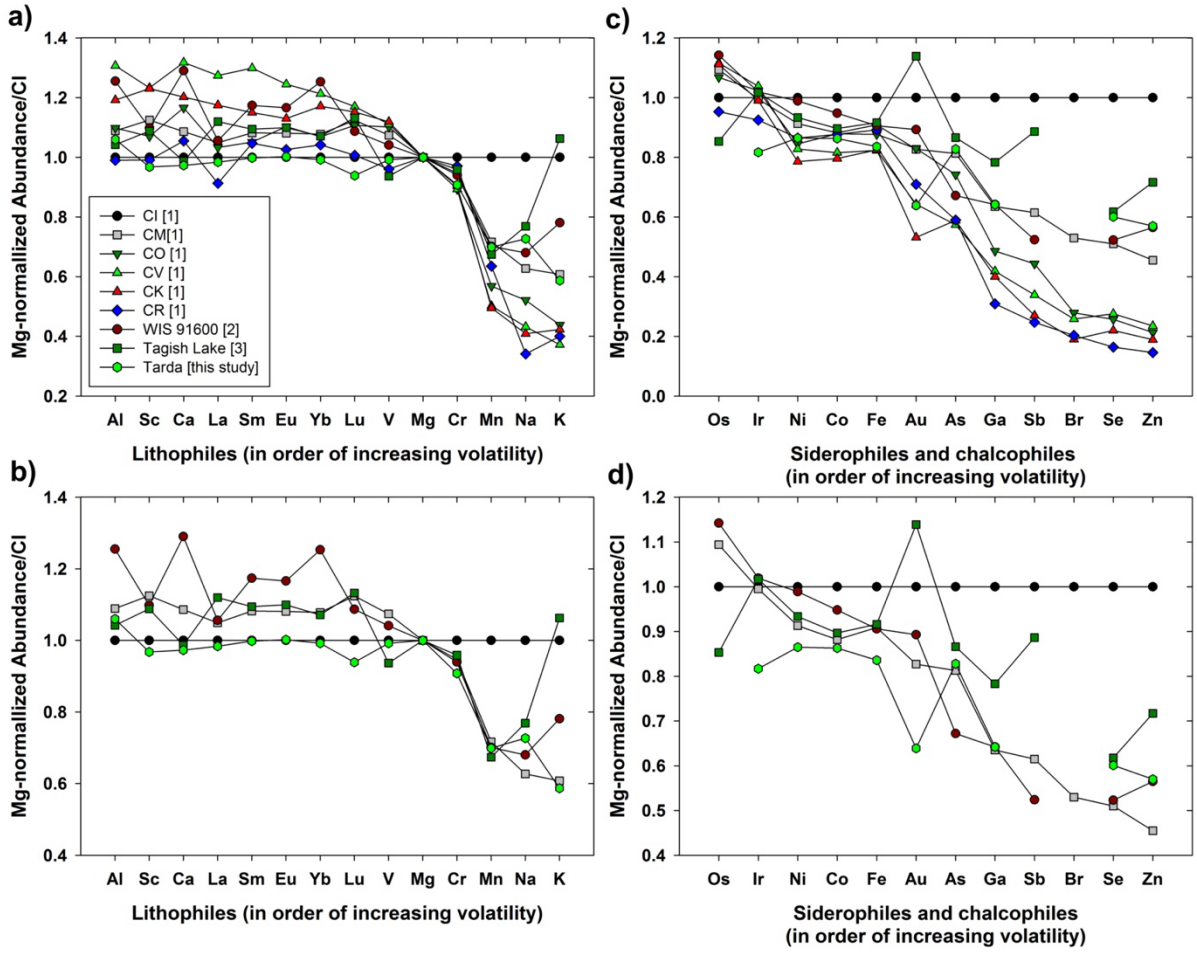

Figure 8. Bulk elemental composition "spider diagrams" showing the chemical differences between the CI, CM, CO, CV, CK and CR chondrites ([1] Lodders et al., 2021), compared to WIS 91600 ([2] Choe et al., 2010), Tagish Lake ([3] Brown et al., 2000), and Tarda (this study). (a, b) Mg- and CI-normalized abundances of lithophile elements in (a) the Tagish Lake-like meteorites compared established meteorite groups and (b) only CI and CM chondrites. (c, d) Mg- and CI-normalized abundances of siderophile and chalcophile elements in (c) the Tagish Lake-like meteorites compared to established meteorite groups and (d) only CI and CM chondrites. Elements are ordered by volatility (50% condensation temperatures; Lodders, 2021).

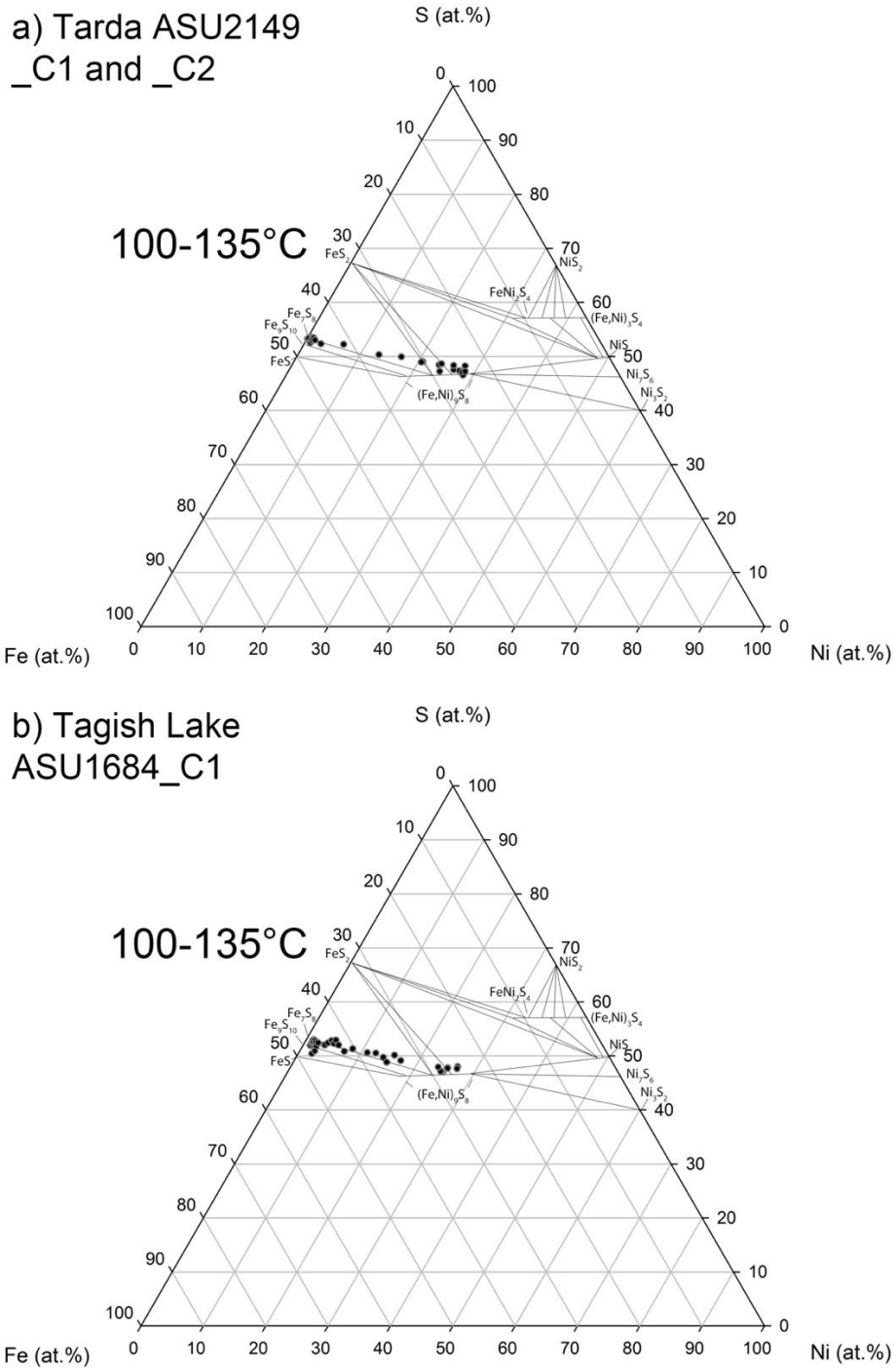

Figure 9. Fe–Ni–S (at.%) ternary phase diagrams that most closely match the sulfide compositions in (a) Tarda ASU2149_C1 and _C2, and (b) Tagish Lake ASU1684_C1. Sulfide compositions are consistent with equilibration between 100 °C and 135 °C; pentlandite in each sample is near the pentlandite stability field and pyrrhotite is along the tie line between pyrrhotite and the pentlandite field. Phase diagrams adapted from Raghavan (2004) with original data from Naldrett (1989) (100–135 °C).

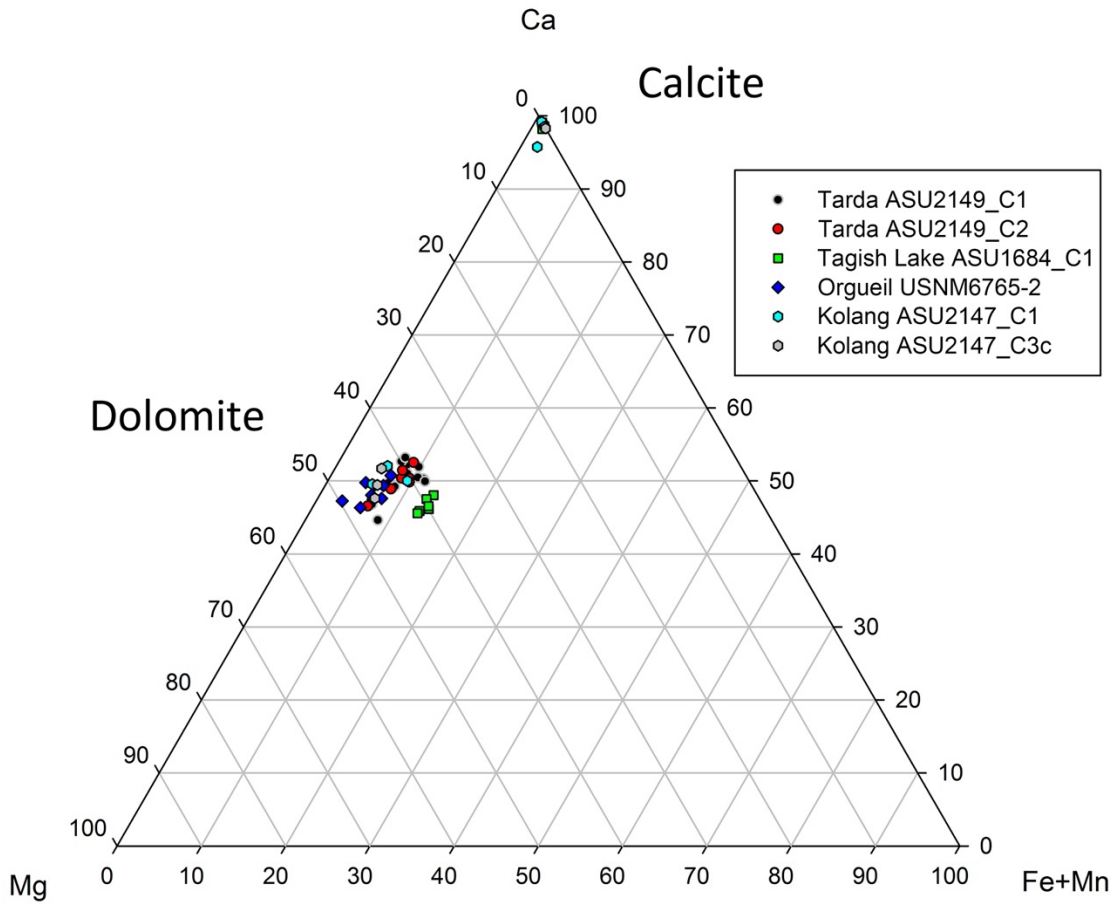

Figure 10. Fe+Mn–Ca–Mg (mol.%) ternary diagram of carbonates in Tarda ASU2149_C1 and _C2 (C2-ung), Tagish Lake ASU1684_C1 (C2-ung), Orgueil USNM6765-2 (CI), Kolang ASU2147_C1 (CM1/2), and Kolang ASU2147_C3c (CM1 clast). Most carbonates analyzed were dolomite, but calcite was also observed in Kolang and Tagish Lake.

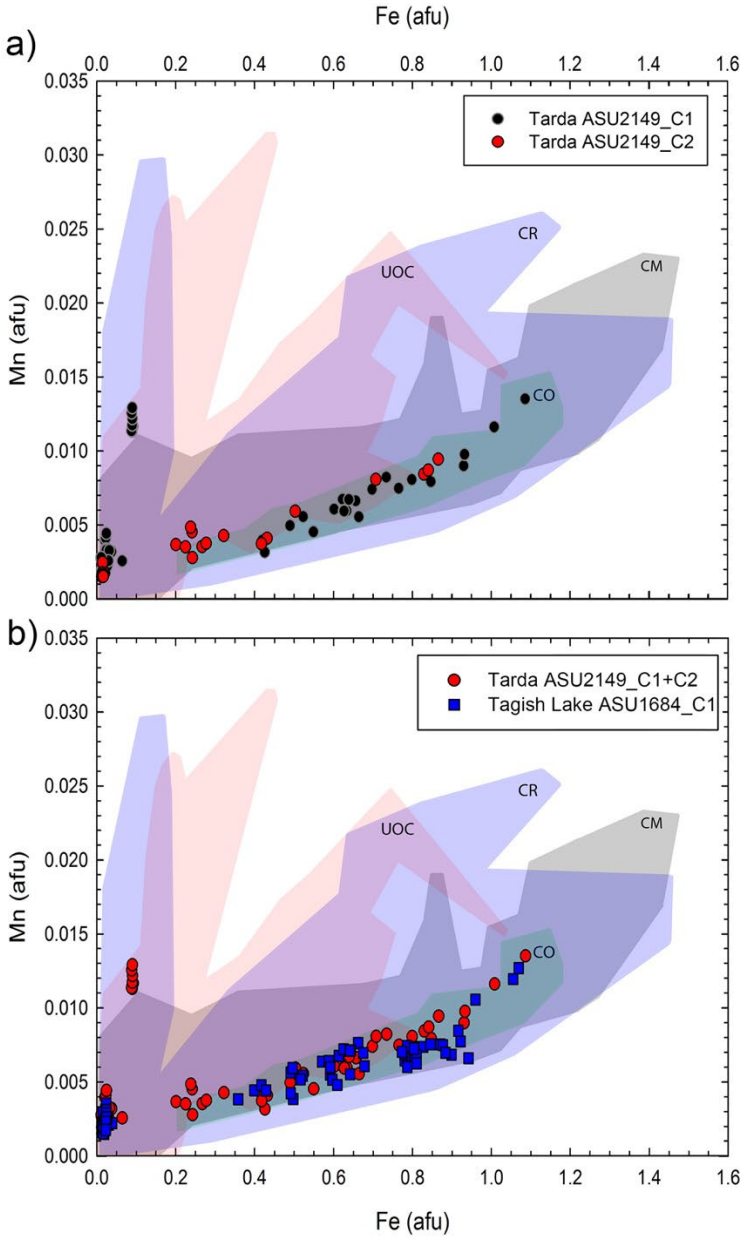

Figure 11. Fe vs. Mn (atomic formula unit or afu) compositions of chondrule olivine from (a) Tarda with _C1 and _C2 separated with black and red, and (b) Tarda vs. Tagish Lake vs. chondrite compositional fields (2 block). Compositional ranges of chondrules are shown for CR (Berlin et al., 2011; Schrader et al., 2015), CO (Jones, 1992; Berlin et al., 2011), CM (Schrader and Davidson, 2017) chondrites, and unequilibrated ordinary chondrites or UOCs (Jones, 1990; Berlin et al., 2011; Schrader and Davidson, 2022).

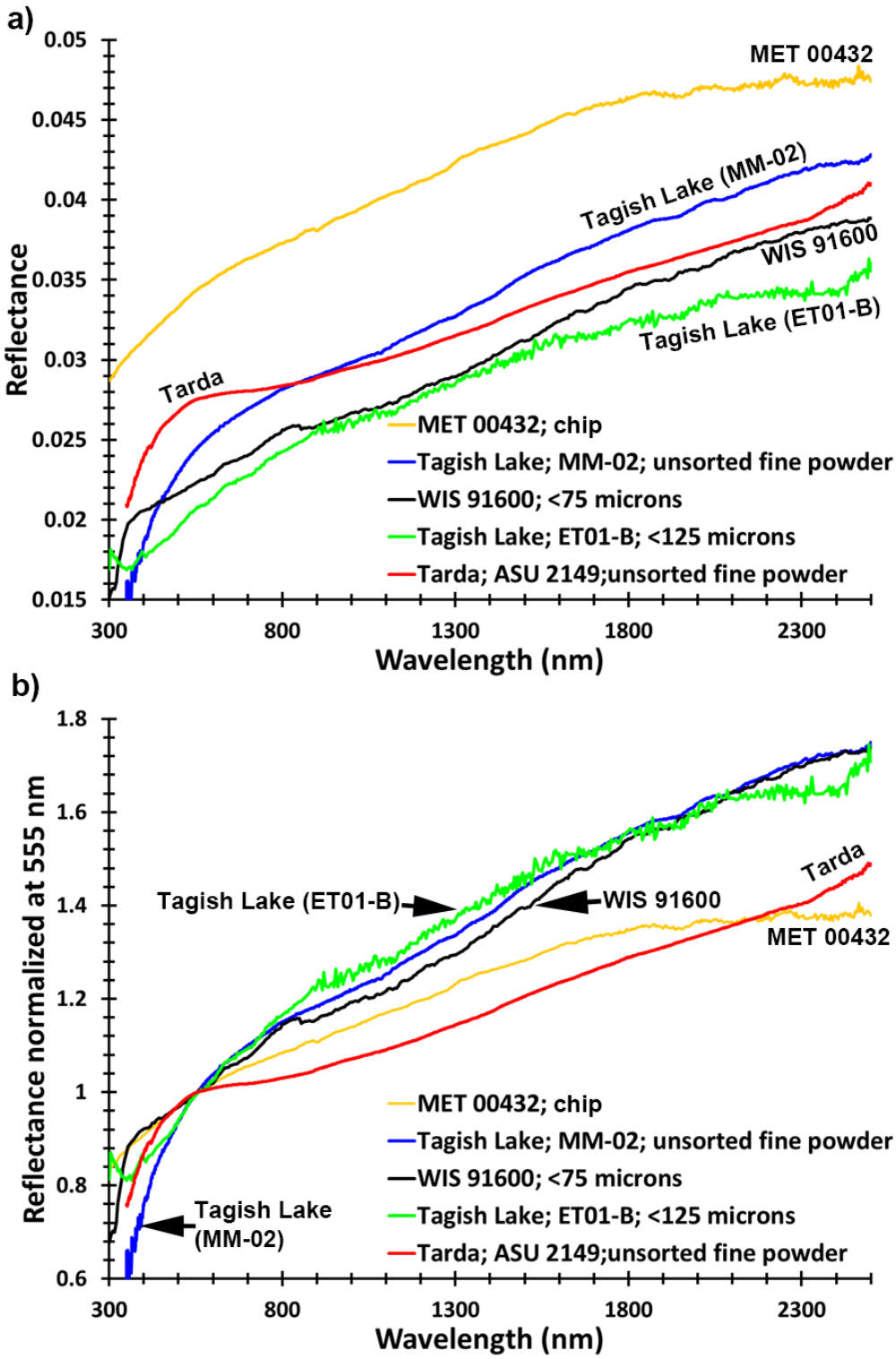

Figure 12. Reflectance spectra of the Tarda (measured at C-TAPE), WIS 91600 and Tagish Lake (measured at RELAB), and MET 00432 (measured at Mizusawa VLBI Observatory) meteorites. These are the few meteorite spectra that are most similar to Tarda in terms of low albedo, red spectral slope, and weak or non-existent absorption bands. a) absolute reflectance. b) spectra normalized to one at 555 nm. See text for details.

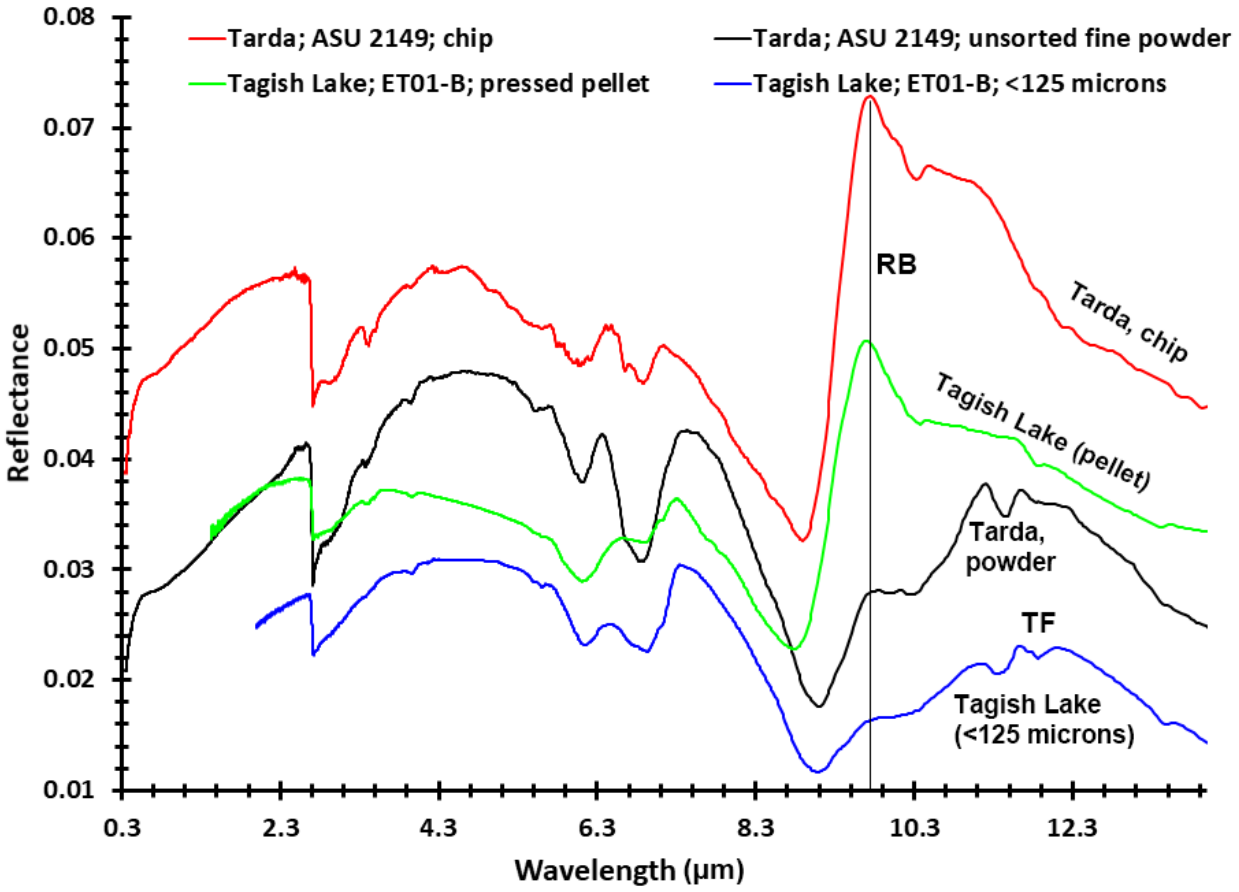

Figure 13. Reflectance spectra of the Tarda chip and powder, Tagish Lake pressed pellet and powder. The vertical line near 9.80 μm shows location of the reststrahlen band (RB) and a transparency feature (TF) is labeled at 11.5 μm. See text in §4.1.6. for details.

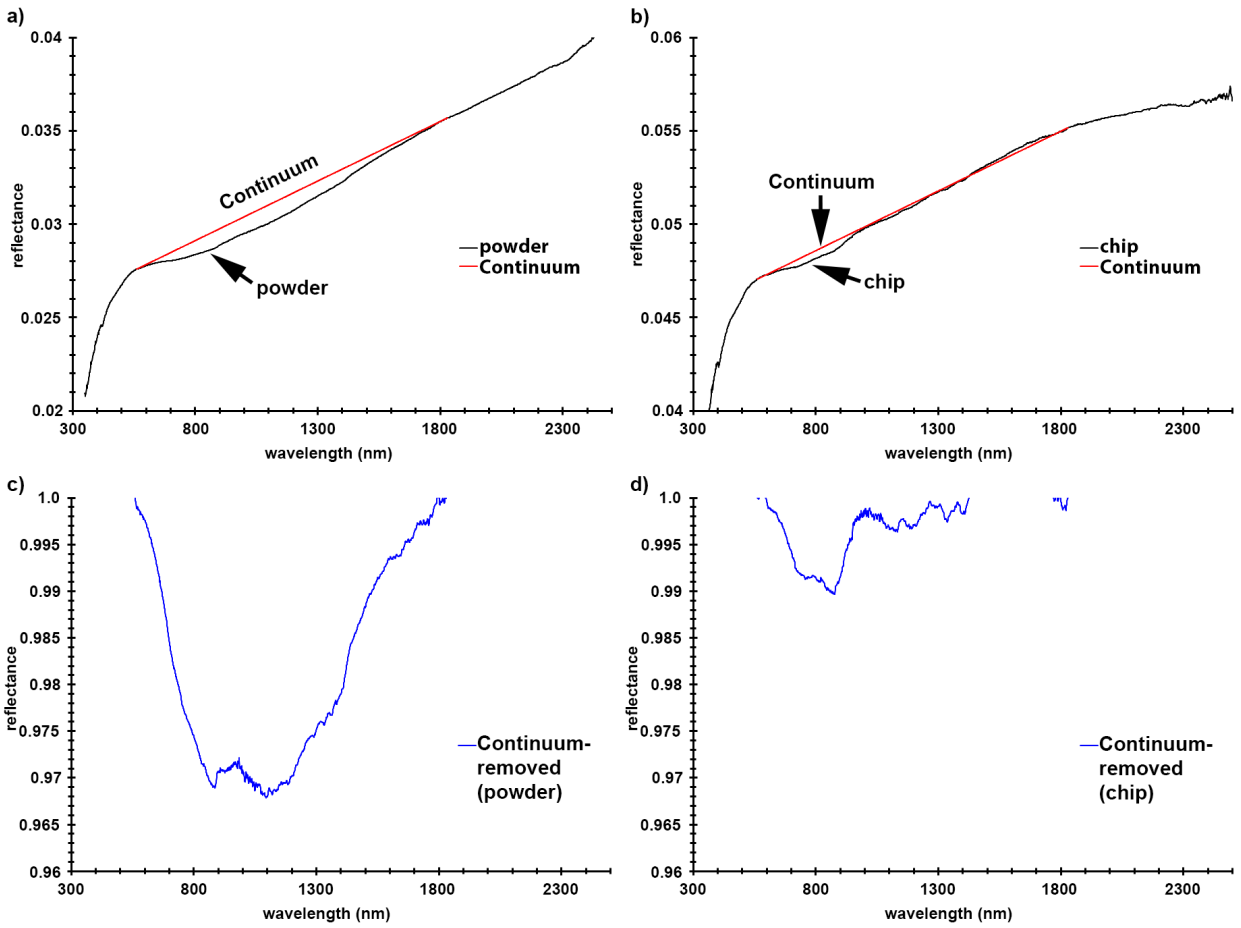

Figure 14. Reflectance spectra of the Tarda powder (a) and chip (b), showing straight line continua (red lines), used to isolate absorption features in the ~500–1800 nm region. Continuum-removed spectra of the powder (c) and chip (d). See text for details.

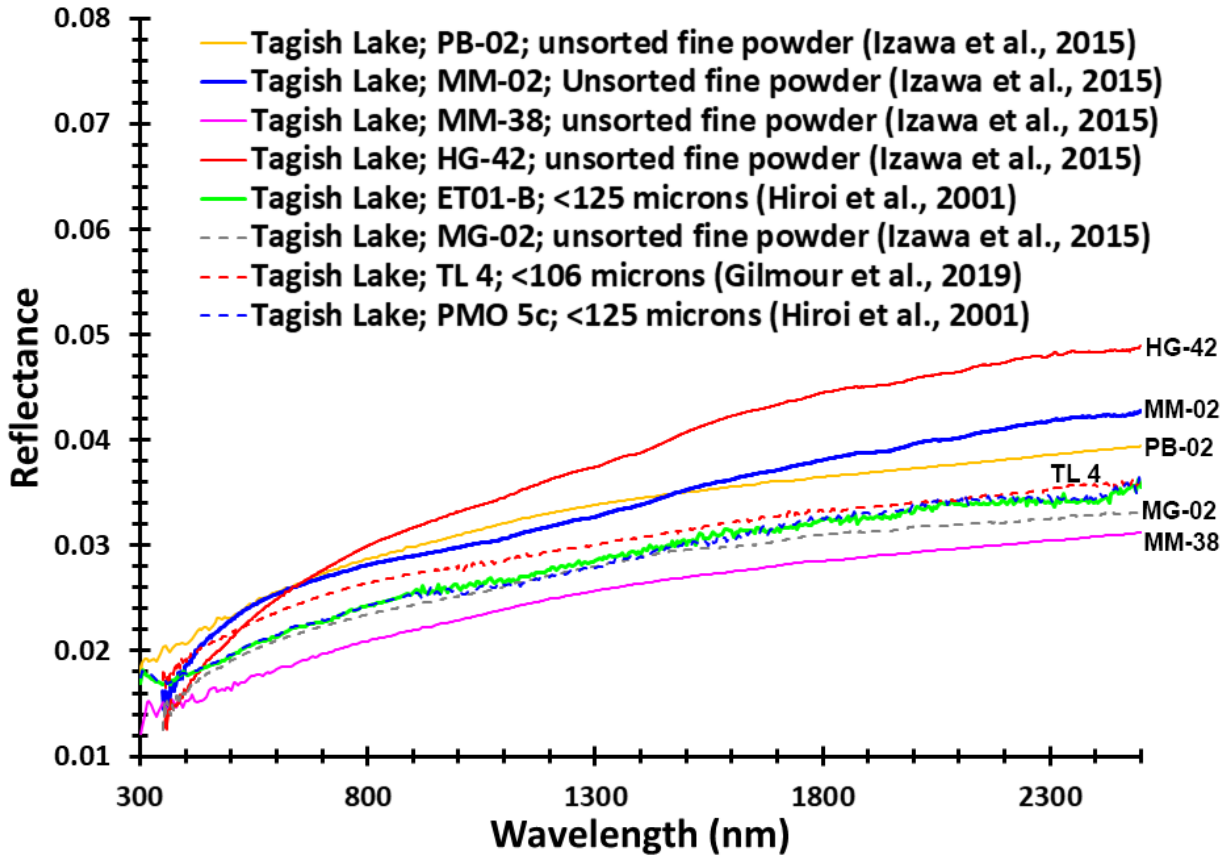

Figure 15. Reflectance spectra of various subsamples of the Tagish Lake meteorite, showing diversity of spectral slopes. The spectra are from the RELAB archive and C-TAPE.

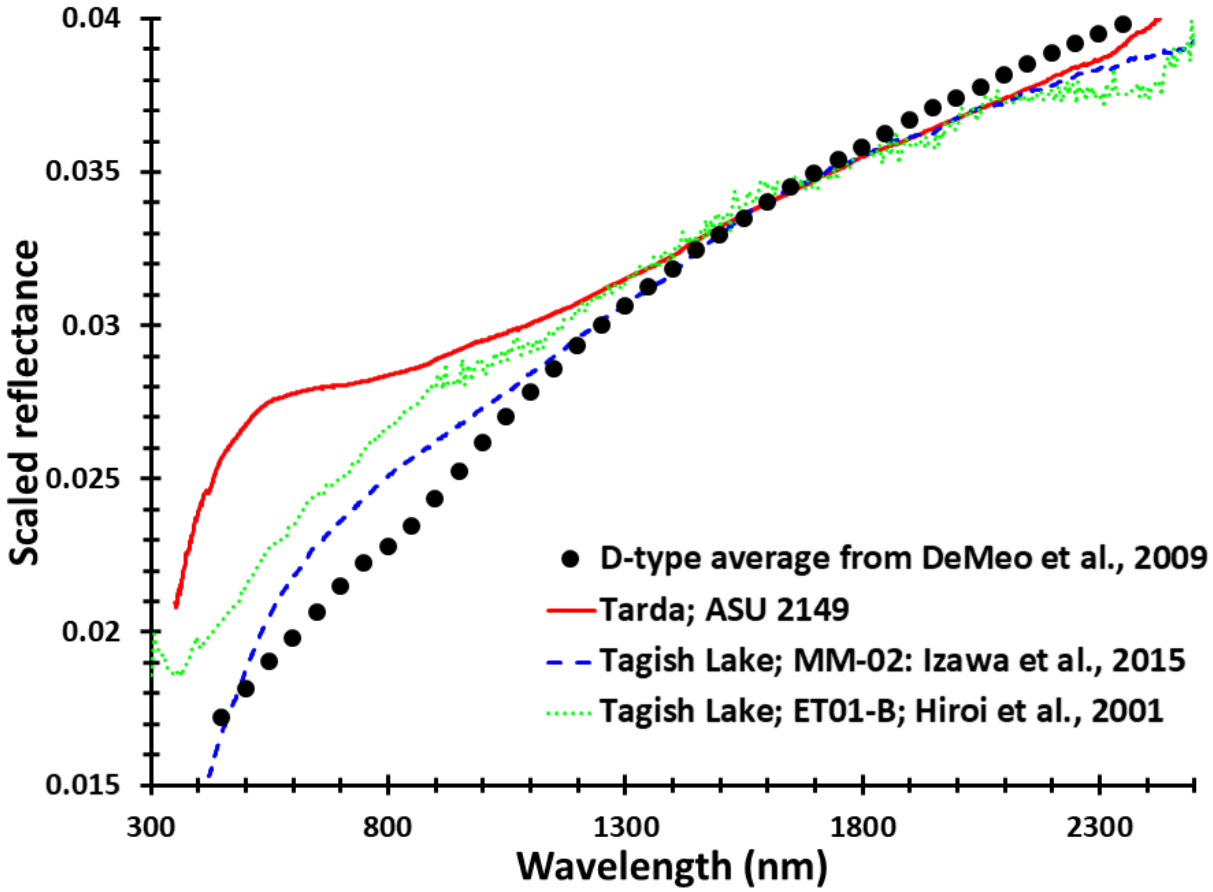

Figure 16. Comparison of the Tarda unsorted fine powder spectrum to an average of D-type asteroids (from DeMeo et al., 2009), as well as Tagish Lake powder (Hiroi et al. 2001; Izawa et al., 2015). The D-type asteroid spectra average has been multiplied by 0.019 to match the Tarda spectrum at 1600 nm. This was done to account for the lack of absolute reflectance for most D-type asteroids.

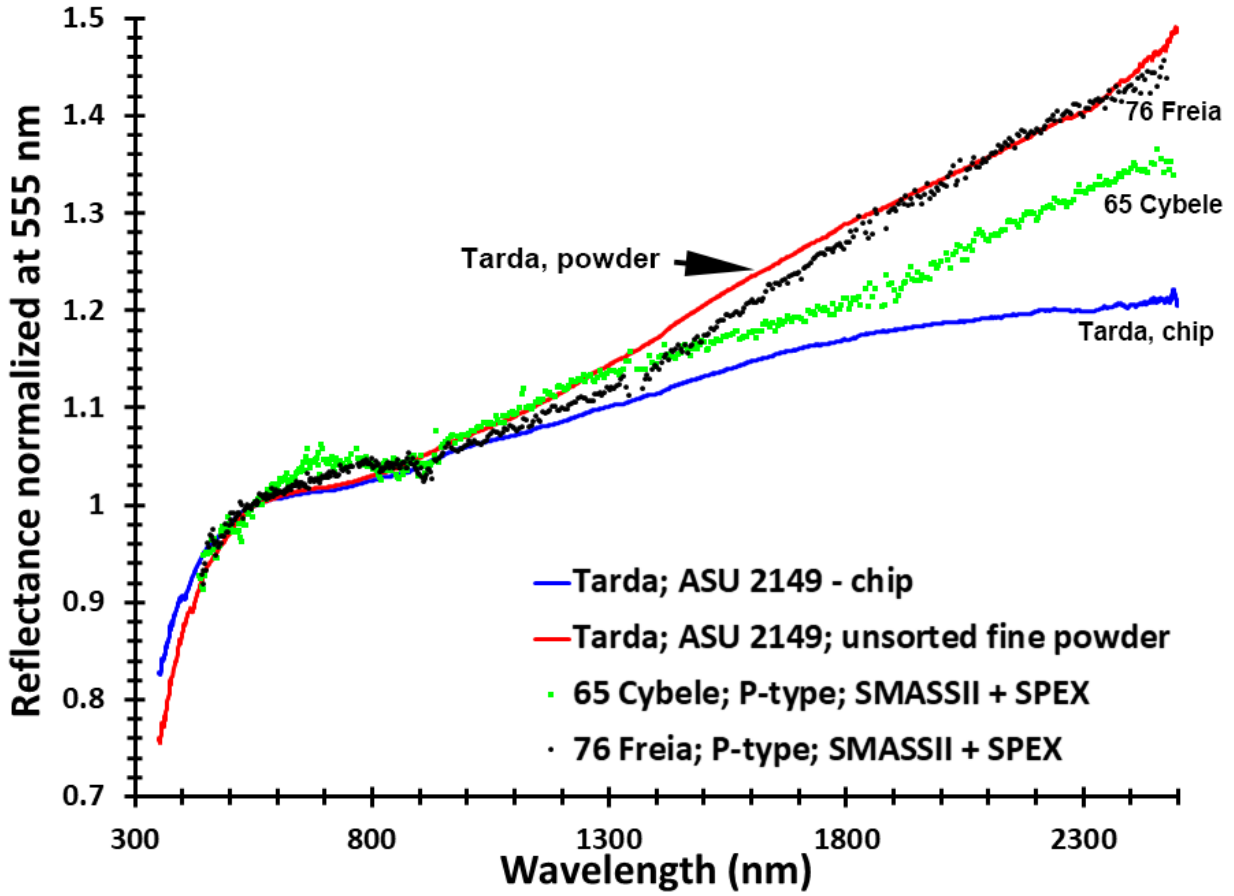

Figure 17. Comparison of normalized reflectance spectra of the Tarda chip and powder spectra to two spectral P-type asteroids (65 Cybele and 76 Freia, data from: Bus and Binzel, 2002b; Burbine and Binzel, 2002; Rayner et al., 2003).